Inorganic Chemistry

Article

pubs.acs.org/IC

# Electrochemiluminescent Monomers for Solid Support Syntheses of Ru(II)-PNA Bioconjugates: Multimodal Biosensing Tools with Enhanced Duplex Stability

Tanmaya Joshi,[†] Gregory J. Barbante,[‡] Paul S. Francis,[‡] Conor F. Hogan,[§] Alan M. Bond,[†] Gilles Gasser,*[,⊥] and Leone Spiccia*[,†]

[†]ARC Centre of Excellence for Electromaterials Science and School of Chemistry, Monash University, Clayton, Victoria 3800, Australia

[‡]School of Life and Environmental Sciences, Deakin University, Geelong, Victoria, 3217, Australia

[§]Department of Chemistry, La Trobe Institute for Molecular Science, La Trobe University, Victoria, 3086, Australia

[⊥]Institute of Inorganic Chemistry, University of Zurich, Winterthurerstrasse 190, CH-8057 Zurich, Switzerland

Supporting Information

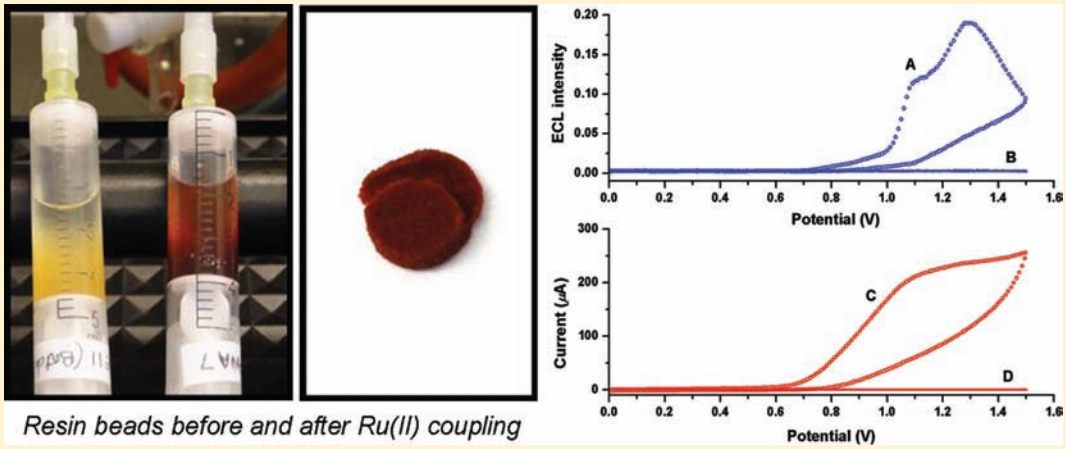


Resin beads before and after Ru(II) coupling

**ABSTRACT:** The feasibility of devising a solid support mediated approach to multimodal Ru(II)-peptide nucleic acid (PNA) oligomers is explored. Three Ru(II)-PNA-like monomers, $[Ru(bpy)_2(Cpp\text{-}L\text{-}PNA\text{-}OH)]^{2+}$ (**M1**), $[Ru(phen)_2(Cpp\text{-}L\text{-}PNA\text{-}OH)]^{2+}$ (**M2**), and $[Ru(dppz)_2(Cpp\text{-}L\text{-}PNA\text{-}OH)]^{2+}$ (**M3**) (bpy = 2,2′-bipyridine, phen = 1,10-phenanthroline, dppz = dipyrido[3,2-*a*:2′,3′-*c*]phenazine, Cpp-L-PNA-OH = [2-(*N*-9-fluorenylmethoxycarbonyl)aminoethyl]-*N*-[6-(2-(pyridin-2yl)-pyrimidine-4-carboxamido)hexanoyl]-glycine), have been synthesized as building blocks for Ru(II)-PNA oligomers and characterized by IR and $^1$H NMR spectroscopy, mass spectrometry, electrochemistry and elemental analysis. As a proof of principle, **M1** was incorporated on the solid phase within the PNA sequences H-g-c-a-a-t-a-a-a-a-Lys-$NH_2$ (**PNA1**) and H-P-K-K-K-R-K-V-g-c-a-a-t-a-a-a-a-lys-$NH_2$ (**PNA4**) to give **PNA2** (H-g-c-a-a-t-a-a-a-a-***M1***-lys-$NH_2$) and **PNA3** (H-P-K-K-K-R-K-V-g-c-a-a-t-a-a-a-a-***M1***-lys-$NH_2$), respectively. The two Ru(II)-PNA oligomers, **PNA2** and **PNA3**, displayed a metal to ligand charge transfer (MLCT) transition band centered around 445 nm and an emission maximum at about 680 nm following 450 nm excitation in aqueous solutions (10 mM PBS, pH 7.4). The absorption and emission response of the duplexes formed with the cDNA strand (**DNA**: 5′-T-T-T-**T-T-T-T-A-T-T-G-C**-T-T-T-3′) showed no major variations, suggesting that the electronic properties of the Ru(II) complexes are largely unaffected by hybridization. The thermal stability of the **PNA·DNA** duplexes, as evaluated from UV melting experiments, is enhanced compared to the corresponding nonmetalated duplexes. The melting temperature ($T_m$) was almost 8 °C higher for **PNA2·DNA** duplex, and 4 °C for **PNA3·DNA** duplex, with the stabilization attributed to the electrostatic interaction between the cationic residues (Ru(II) unit and positively charged lysine/arginine) and the polyanionic DNA backbone. In presence of tripropylamine (TPA) as co-reactant, **PNA2**, **PNA3**, **PNA2·DNA** and **PNA3·DNA** displayed strong electrochemiluminescence (ECL) signals even at submicromolar concentrations. Importantly, the combination of spectrochemical, thermal and ECL properties possessed by the Ru(II)-PNA sequences offer an elegant approach for the design of highly sensitive multimodal biosensing tools.

**Received:** December 23, 2011
**Published:** February 16, 2012

## INTRODUCTION

Since their advent, peptide nucleic acids (PNA)[1] have shown evolving importance in various multidisciplinary areas of research. These artificial DNA analogues are considered excellent candidates for biological applications.[2] Their high affinity for cDNA/RNA, stability toward proteases and nucleases, and ability to distinguish single base mismatches make them suitable for antigene and antisense applications.[2] To expand the scope for application of these inherent capabilities of PNAs, structural modifications have been made to their backbone. Examples of such modifications span from replacing the natural bases with unnatural nucleobases to the introduction of fluorescent and/or electrochemical labels.[2−12] While the fluorophore-labeled PNAs have been widely used as diagnostic probes for nucleic acid sequences (e.g., PNA-FISH assay)[13−15] and for fluorescence-based cellular uptake studies aimed at antisense applications,[2,7,16−18] electrochemical labels were introduced with the aim of using them as electrochemical biosensors.[7−9,19−21] Ferrocene has been most widely employed for these purposes because of the stability of the ferrocenyl group, accessibility of a large library of its derivatives, and favorable electrochemical properties.[22] Numerous examples of ferrocene conjugated PNA monomers and sequences are available in literature.[3,7,8,21,23−25] However, the absence of any photophysical activity limits its scope in biosensing to electroactive probes. Recently, Gasser, Metzler-Nolte, and coworkers have emphasized the advantages of increasing the versatility of PNA conjugates by introducing multiple detection labels on the same PNA backbone.[24,26−28] They employed "click chemistry" to build different PNA monomers and oligomers incorporating ferrocene as electroactive unit[24,29,30] and have also demonstrated the feasibility of introducing multiple organometallic moieties into the same PNA oligomer using solid phase synthesis.[24,28,30]

Ruthenium(II)-polypyridyl complexes possess a wide array of tunable photophysical, electrochemical, chemiluminescent, and electrochemiluminescent (ECL) properties.[31−38] Their high chemical, thermal and photochemical stability, reversible redox behavior, substantial UV−visible absorption, and long-lived metal to ligand charge transfer (MLCT) excited states make them suitable for use as electroactive/photoactive biosensing probes.[32,36−40] In addition to intense visible light absorption, ruthenium(II)-polypyridyl complexes also possess a large Stokes shift, making them particularly useful for the in vitro study of biological processes.[35,40] The mechanistic intricacies of cellular uptake for ruthenium polypyridyl complexes have been closely investigated by Barton and co-workers.[41] The characteristic luminescence of these complexes was exploited in measurements of cellular uptake, using flow cytometry and confocal microscopy.[41] It has also been demonstrated that these complexes can be transported inside living cells.[41] The lipophilicity of the ligands has been proposed as one of the factors governing cellular uptake, in agreement with independent studies on the cellular uptake of transition metal complexes.[41] Numerous conjugation strategies, such as highly positively charged short peptide sequences, nuclear localization sequences (NLSs), and cell penetrating peptides (CPP), have been employed to improve the cellular uptake and localization of these complexes inside the cell.[41,42] These studies indicate that ruthenium polypyridyl complexes are excellent choices as labels to be introduced on the PNA backbone, as they can influence the cellular uptake in addition to serving as detection tools.[41,42] Metzler-Nolte and co-workers have reported the synthesis of Ru(II) conjugated PNA oligomers.[43] The metal complex was attached via an amide bond at the *N*-terminal of the PNA heptamer following solid phase synthesis protocols.[43] To address the limitations associated with such a *N*-terminal PNA insertion of the Ru(II) complexes, we recently reported the synthesis of the Ru(II) based PNA-like monomers.[44,45] These monomers objectively addressed some synthetic limitations associated with preparation of similar $Ru^{II}$−PNA oligomers by allowing solid phase synthesis to be used for the introduction of the metal complex at any chosen location in the PNA sequence.[44,45] Use of these Ru(II)-PNA-like monomers thus overcomes the otherwise inevitable loss of the reactive terminal amino group of PNA. This has previously prevented further modification of the PNA through the systematic conjugation of peptide moieties promoting cellular uptake at the *N*-terminus.[2,43,46]

Herein, we report the synthesis of novel Ru(II) polypyridyl PNA-like monomers **M1**, **M2**, and **M3** as racemic mixtures (Figure 1) and characterization of their photoluminescence, electrochemical, and ECL properties. The bidentate ligand 2-(2′-pyridyl)pyrimidine-4-carboxylic acid (CppH), bearing a single carboxylate functionality, is used to bypass the difficulties in preparation and purification of the commonly used Mebpy-COOH ligand. The three monomers differ from each other in terms of the ancillary diimine ligands, that is, bis(bipyridyl) vs bis(phenanthroline) vs bis(dipyridophenazine). We illustrate

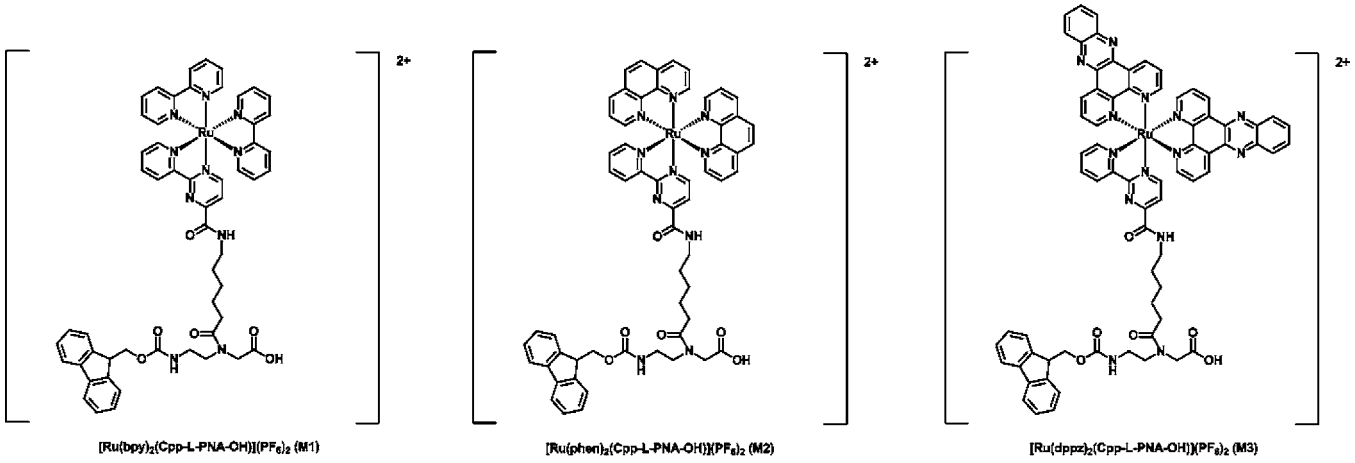


**Figure 1.** Structure of Ru(II)-PNA monomer complexes, **M1**−**M3**.


dx.doi.org/10.1021/ic202761w | *Inorg. Chem.* 2012, 51, 3302−3315

the successful solid support insertion of monomer **M1** within the PNA oligomeric sequence. To the best of our knowledge, it is the first example of intrasequence labeling of a PNA sequence with the Ru(II) complex via solid phase synthesis. The synthesis of Ru(II)-PNA oligomers has been further complemented with thermal melting, photoluminescence, and ECL studies exploring their interactions with cDNA sequences.

## EXPERIMENTAL SECTION

**Chemicals.** Chemicals were either of reagent or analytical grade and used as purchased from commercial sources, unless otherwise stated. Analytical grade solvents were degassed by purging with dry, oxygen-free nitrogen for at least 30 min before use if necessary. Acetonitrile was dried before use by standing over calcium hydride overnight. Deionized water was used for all reactions in aqueous solution. HPLC grade solvents were used for all spectral studies. Tetrabutylammonium hexafluorophosphate ($nBu_4NPF_6$, Fluka) was recrystallized prior to use as the electrolyte for the electrochemical studies in acetonitrile.[47] Deionized water (18 MΩ.cm) and/or acetonitrile were used for rinsing the electrochemical glass cell throughout the experiments. Phosphate Buffered Saline (PBS) tablets for preparing phosphate buffer (10 mM, pH 7.4) were purchased from Sigma, and the buffer solution was reconstituted in nanopure water. Reagents and solvents for solid phase peptide synthesis were of HPLC grade and purchased from Acros (Geel, Belgium), Aldrich/Sigma/Fluka (Deisenhofen, Germany), E. Merck (Darmstadt, Germany), and IRIS Biotech (Marktredwitz, Germany) and were used without further purification. The preloaded polystyrene resins were purchased from Rapp Polymers (Tübingen, Germany). Only L-amino acids were used throughout. PNA monomers were purchased from Link Technologies (Edinburgh, Scotland). DNA oligonucleotide (5′-T-T-T-T-T-T-T-A-T-T-G-C-T-T-T-3′) was custom-synthesized by Micromon, Monash University (Victoria, Australia).

**Instrumentation and Methods.** A vacuum line and Schlenk glassware were employed when reactions had to be carried out under an atmosphere of dry, oxygen-free nitrogen. Where necessary the reaction vessels were protected from light by wrapping them with aluminum foil. $^1H$ and $^{13}C$ NMR spectra were measured on Bruker AC200, AM300, or DRX 400 spectrometers using the signal of the deuterated solvent as an internal standard. The chemical shifts $\delta$ are reported in parts per million (ppm) relative to tetramethylsilane (TMS) or signals from the residual protons of deuterated solvents.[48] Coupling constants, $J$, are given in hertz (Hz). Peak multiplicities are abbreviated as follows: s (singlet), d (doublet), t (triplet), and m (multiplet). Electrospray ionization (ESI) mass spectrometry was performed using a Micromass Platform *II* mass spectrometer fitted with an ESI source (capillary voltage was 3.5 eV and the cone voltage 35 V). The most intense peak is listed. Accurate high-resolution mass spectra were recorded with a Bruker BioApex II 47e FT-ICR MS fitted with an Analytica Electrospray Source. Samples were introduced by a syringe pump at a rate of 1 $\mu$L min$^{-1}$, and the capillary voltage was at 200 V. The matrix-assisted laser desorption/ionization time-of-flight mass spectrometry (MALDI-TOF) mass spectra were measured on a Bruker Daltonics Autoflex. The experiments were performed in either linear or reflector mode with positive polarity using sinapinic acid or $\alpha$-cyano-4-hydroxy-cinnamic acid as the matrix. Infrared spectra were recorded on a Perkin-Elmer 1600 Series FTIR spectrometer in the range 4000−500 cm$^{-1}$ with a resolution of ±4.0 cm$^{-1}$. Samples were measured as KBr disks or neat as indicated. Peak intensities are given as broad (b), very strong (vs), strong (s), medium (m), and weak (w). Microanalyses were carried out by the Campbell Microanalytical Laboratory, University of Otago, New Zealand. UV/visible spectra were recorded using Varian Cary Bio 300 or 5G spectrophotometers. Emission spectra were obtained following excitation at 450 nm on a Fluoromax-4 spectrofluorometer (Horiba Jobin Yvon Inc.) and were corrected for instrumental response using manufacturer provided correction factors. Both UV/visible and emission spectra were measured using a 10 $\mu$M acetonitrile solution of each complex at 25 °C in 1 cm quartz cuvettes. The excitation and emission slit width were set to 3.0 and 2.5 nm, respectively, for recording the emission spectra of the complexes. The slit width was increased to 5.0 nm for excitation and 3.5 nm for emission for collecting the emission data for Ru(II)-PNA and Ru(II)-**PNA·DNA** oligomers. UV melting experiments were performed with Varian Cary Bio 100 spectrophotometer equipped with a 6 × 6 multicell block and Peltier thermostat. Circular dichroism (CD) spectra of DNA were recorded at room temperature on a Jasco J-815 spectropolarimeter using one cm quartz cuvettes. Thin layer chromatography (TLC) was performed using silica gel 60 F-254 (Merck) plates with detection of spots being achieved by exposure to iodine or UV light or by using ninhydrin stain. Column chromatography was carried out using silica gel 60 (0.040−0.063 mm mesh, Merck). Eluent mixtures are expressed as volume to volume (v/v) ratios. HPLC purification of PNAs was performed on a Varian ProStar system equipped with a diode array UV/visible spectrometer and a LiChroCART 250−10 RP-18 semiprep column (5 $\mu$m particle size, 100 Å pore size, 10 × 250 mm. Flow rate: 4 mL min$^{-1}$). Chromatographic separations were performed with a linear gradient of A (distilled water containing 0.1% v/v TFA) and B (acetonitrile (Sigma−Aldrich HPLC grade), containing 0.1% v/v TFA). Preparative runs: $t$ = 0 min, 5% B; $t$ = 12 min, 15% B; $t$ = 32 min, 40% B; $t$ = 50 min, 80% B; $t$ = 51 min, 100% B; $t$ = 56 min, 100% B; $t$ = 61 min, 5% B. The LC-MS spectrum of PNA sequences was measured on an Acquity from Waters system equipped with a PDA detector and an auto sampler using an Agilent Zorbax 300SB-C18 analytical column (3.5 mm particle size, 300 Å pore size, 150 × 4.6 mm). The LC was coupled to an Esquire HCT from Bruker (Bremen, Germany) for the MS measurements. The LC run (flow rate: 0.3 mL min$^{-1}$) was performed with a linear gradient of A (distilled water containing 0.1% v/v formic acid) and B (acetonitrile (Sigma−Aldrich HPLC-grade), containing 0.1% v/v formic acid); $t$ = 0 min, 5% B; $t$ = 3 min, 5% B; $t$ = 17 min, 100% B; $t$ = 20 min, 100% B; $t$ = 25 min, 5% B.

**Electrochemical Measurements.** Cyclic voltammetric measurements were performed at (20 ± 2)°C in acetonitrile solutions containing 0.1 M $nBu_4NPF_6$ as the supporting electrolyte over the scan rate range of 100−1000 mV s$^{-1}$ using a BAS 100B (Bioanalytical Systems) electrochemical workstation. Solutions used in electrochemical measurements were deoxygenated by purging with high purity nitrogen for at least 10 min before commencing the experiments. A conventional three electrode cell was employed which comprised a glassy carbon working electrode (area = 0.0079 cm$^2$), a large surface area Pt counter electrode and an Ag/Ag$^+$ (0.1 M $AgNO_3$ in acetonitrile) reference electrode. The potential of the Ag/Ag$^+$ reference electrode was frequently calibrated against that of ferrocene/ferrocinium ($Fc^{0/+}$) redox couple under the conditions used for the voltammetric measurements on the Ru(II) complexes. The working electrode was polished with an aqueous slurry of aluminum oxide (0.3 $\mu$m), then rinsed with acetone and dried before each voltammetric experiment.

ECL experiments were performed using a PGSTAT 12 autolab electrochemical workstation (MEP Instruments, North Ryde, NSW, Australia) or $\mu$AUTOLAB type II potentiostat (MEP Instruments, North Ryde, NSW, Australia) (in case of Ru(II)-PNA and Ru(II)-PNA·DNA oligomers) in combination with General Purpose Electrochemical Systems (GPES) software (version 4.9). In these studies, the electrochemical cell consisted of a glass cell with a quartz base. The cell was enclosed in a custom-built light-tight Faraday cage. A three-electrode configuration consisting of a 3 mm diameter glassy carbon working electrode shrouded in Teflon (CH Instruments, Austin, TX, U.S.A.), a 1 cm$^2$ platinum gauze auxiliary electrode and a silver wire quasi reference electrode was used.

For the non-oligomeric Ru(II) complexes, ECL spectra were obtained using Ocean Optics CCD spectrometer, model QE65000, coupled to the cell with a one meter fiber optic cable. The spectral acquisition was triggered simultaneously with the electrochemical experiment with the aid of a HR 4000 breakout box (Ocean Optics). All complex solutions were prepared at a concentration of 0.1 mM in freshly distilled acetonitrile with 0.1 M $nBu_4NPF_6$ as the supporting electrolyte and 0.1 M tripropylamine as the ECL co-reactant. Solutions of annealed Ru(II)-**PNA·DNA** duplexes and Ru(II)-PNA oligomers


dx.doi.org/10.1021/ic202761w | *Inorg. Chem.* 2012, 51, 3302−3315

were prepared at a concentration of 0.1 $\mu$M in 0.1 M PBS buffer (pH 7.4) and 0.1 M tripropylamine was used as ECL co-reactant. Prior to each experiment, the working electrode was polished sequentially with slurries of 0.3 and 0.05 $\mu$m alumina on a felt pad, sonicated in water (1 min), rinsed in freshly distilled acetonitrile, and dried with a stream of nitrogen. The working electrode was then positioned about 2 mm from the bottom of the cell for detection of the ECL signal, and the solution was purged with argon for 10 min. ECL intensities are given relative to $[Ru(bpy)_3](PF_6)_2$ (100%) measured under the same conditions. To generate the emission, the working electrode was pulsed for 2.0 s between 0 V and a value sufficiently positive to generate the oxidized ruthenium(III) complex in each case. The resulting ECL spectra were collected over the duration of three such chronoamperometric cycles.

**Synthesis.** Compounds 2-(pyridin-2-yl)pyrimidine-4-carboxylic acid·$HNO_3$ (**CppH**) (**1**),[49] dipyrido[3,2-a:2′,3′-c]phenazine (**dppz**),[50] and $[Ru(CO)_2Cl_2]_n$[51] were synthesized according to the literature procedures. The characterization data were in agreement with the published data. Ethyl-6-(2-(pyridin-2-yl)pyrimidine-4-carboxamido)-hexanoate (**2**), 6-(2-(pyridin-2-yl)pyrimidine-4-carboxamido)hexanoic acid (**3**), and *tert*-butyl-*N*-[2-(*N*-9-fluorenylmethoxycarbonyl)-aminoethyl]-*N*-[6-(2-(pyridin-2-yl) pyrimidine-4-carboxamido)-hexanoyl]glycinate (**Cpp-L-PNA**) (**4**) were prepared by procedures to be detailed by us elsewhere.[52]

*$[Ru^{II}(Cpp\text{-}L\text{-}OH)(CO)_2Cl_2]$·MeOH (**5**).* $[Ru(CO)_2Cl_2]_n$ (0.330 g, 1.45 mmol) was suspended in 15 mL of deoxygenated methanol and heated at 60 °C for 15 min to ensure its complete dissolution. 6-(2-(Pyridin-2-yl)pyrimidine-4-carboxamido)hexanoic acid (**3**) (0.503 mg, 1.6 mmol) was added to the resulting clear yellow solution and the reaction mixture refluxed under nitrogen for 2 h, resulting in formation of a yellow precipitate. The reaction mixture was cooled to 2 °C overnight for complete precipitation of the product which was collected by filtration, and washed with ether and ice-cold methanol to obtain **5** as a yellow solid. Yield: 0.667 g (85%). Anal. Calcd. for $C_{19}H_{22}Cl_2N_4O_6Ru$ (%): C, 39.73; H, 3.86; N, 9.75. Found (%): C, 39.94; H, 3.88; N, 9.82. IR (KBr): $\nu$ 3330s (N−H), 3082m (C−$H_{arom}$), 2941s (C−$H_{aliph}$), 2079vs (C≡O), 2015vs (C≡O), 1718s (C═O), 1675s (C═O), 1588m, 1528s, 1437w, 1412m, 1282w, 1201m, 1061w, 866m, 820m, 765s, 700, 663w, 629m $cm^{-1}$. $^1H$ NMR (300 MHz, DMSO-$d_6$): $\delta$ 9.77 (d, $^3J$ = 5.7 Hz, 1H), 9.57−9.53 (m, 1H), 9.34−9.28 (m, 2H), 8.54−8.49 (m, 1H), 8.29 (d, $^3J$ = 6.0 Hz, 1H), 8.06−8.01 (m, 1H), 2.22 (t, $^3J$ = 7.2 Hz, 2H), 1.67−1.51 (m, 4H), 1.41−1.32 (m, 2H) ppm. Two proton signals are masked by residual water from DMSO-$d_6$. MS ($ESI^+$): $m/z$ 542.9 $[M+H]^+$.

*$[Ru(dppz)_2(Cpp\text{-}L\text{-}OH)](PF_6)_2\cdot 5H_2O$ (**6**).* Dipyrido[3,2-*a*:2′,3′-*c*]-phenazine (**dppz**) (0.520 g, 1.84 mmol) and trimethylamine-N-oxide dihydrate (0.370 g, 3.32 mmol) were added to a solution of $[Ru^{II}(Cpp\text{-}L\text{-}OH)(CO)_2Cl_2]$ (**5**) (0.400 g, 0.74 mmol) in 20 mL of deoxygenated 2-methoxyethanol. The reaction solution was heated to reflux for 4 h under nitrogen. After cooling the solution to room temperature, the solvent was removed on a rotary evaporator to obtain the crude product. The crude product was dissolved in 15 mL of acetonitrile/$H_2O$/conc. $H_2SO_4$ (45:45:10) and refluxed for 24 h. Acetonitrile was removed by rotary evaporation, and the residue was diluted with 10 mL distilled water. An aqueous solution of $HPF_6$ (60%) was added dropwise until no further precipitation was observed. The orange precipitate collected by filtration was dissolved in ethanol/acetonitrile (1:1), layered with diethylether, and left to stand at room temperature. The orange solid obtained on standing was collected by filtration and further purified by silica gel column chromatography using acetonitrile/$H_2O$/sat. $KNO_3$ (16:3:1) as eluent. The dark orange band was collected and solvent removed under reduced pressure. The residue obtained was suspended in minimal amount of acetonitrile and filtered to remove insoluble $KNO_3$. The filtrate was evaporated to dryness, and the residue suspended in water. The dropwise addition of $HPF_6$ (60%) completed the precipitation of **5**. The orange solid was collected by filtration, washed with ether, and dried in vacuo. Yield: 0.634 g (68%). Anal. Calcd. for $C_{52}H_{48}F_{12}N_{12}O_8P_2Ru$ (%): C, 45.92; H, 3.56; N, 12.36. Found: C, 45.94; H, 3.71; N, 12.38. IR (KBr): $\nu$ 3450br (O−H), 3333w (N−H), 3085w (C−$H_{arom}$), 2924m (C−$H_{aliph}$), 2862m (C−$H_{aliph}$), 1655br (C═O), 1541w, 1525w, 1433w, 1416m, 1360w, 1230w, 1184m, 1119m, 1077m, 1048w, 844vs, 764m, 725m $cm^{-1}$. $^1H$ NMR (400 MHz, DMSO-$d_6$): $\delta$ 9.70 (d, $^3J$ = 8.4 Hz, 2H), 9.63−9.59 (m, 2H), 9.44 (d, $^3J$ = 8.4 Hz, 1H), 8.70−8.68 (m, 1H), 8.55−8.50 (m, 4H), 8.37 (d, $^3J$ = 6.0 Hz, 2H), 8.33−8.18 (m, 8H), 8.11−8.04 (m, 2H), 7.92−7.61 (m, 4H), 7.61−7.58 (m, 1H), 2.12 (t, $^3J$ = 7.2 Hz, 2H), 1.60−1.53 (m, 4H), 1.36−1.30 (m, 2H) ppm. Two proton signals are masked by residual water from DMSO-$d_6$. MS ($ESI^+$): $m/z$ 490.1 $[M]^{2+}$. HR-ESI mass spectrum (acetonitrile:methanol 1:4): found 490.1122; calcd. for $[C_{52}H_{38}N_{12}O_3Ru]/z$ 490.1117.

*$[Ru(bpy)_2(Cpp\text{-}L\text{-}PNA\text{-}OH)](PF_6)_2\cdot 5H_2O$ (**M1**).* **Cpp-L-PNA** (**4**) (0.970 g, 1.4 mmol) was stirred in a 1:1 solution of TFA/dichloromethane (5 mL) at room temperature for 5 h. The solvent was evaporated under reduced pressure, and the oily residue dissolved in ethanol/$H_2O$ (1:1, 20 mL). The solution was degassed, and $Ru(bpy)_2Cl_2$ (0.566 g, 1.17 mmol) added. The reaction mixture was refluxed under a nitrogenous atmosphere for 5 h, and, after cooling to room temperature, the solvent volume was reduced (ca. 5 mL) by rotary evaporation. The residue was diluted with water (10 mL) and filtered. An aqueous solution of $HPF_6$ (60%) was then added dropwise to the filtrate until no further precipitation was observed. A dark orange solid was obtained which was collected by filtration, washed with water and ether, and dried under high vacuum to obtain PNA monomer **M1**. Yield: 1.35 g (85%). Anal. Calcd. for $C_{55}H_{62}F_{12}N_{10}O_{11}P_2Ru$ (%): C, 46.19; H, 4.37; N, 9.79. Found: C, 46.02; H, 4.46; N, 9.92. IR (Neat): $\nu$ 3450br (O−H), 3085w (C−$H_{arom}$), 2929m (C−$H_{aliph}$), 2863m (C−$H_{aliph}$), 1687m (C═O), 1654m (C═O), 1650m (C═O), 1536m, 1461m, 1441br, 1245m, 1188w, 1161w, 1122w, 1086m, 1016m, 843vs, 763s, 745m, 731m $cm^{-1}$. $^1H$ NMR (400 MHz, $CD_3CN$): $\delta$ 9.13−9.09 (m, 1H), 8.65−8.63 (min) and 8.55−8.50 (maj) (rotamers, m, 4H), 8.17−8.15 (rotamers, m, 1H), 8.11−8.03 (m, 4H), 7.91−7.87 (rotamers, m, 2H), 7.84−7.77 (m, 2H), 7.76−7.71 (m, 4H), 7.62−7.59 (m, 2H), 7.57−7.50 (m, 2H), 7.46−7.35 (rotamers, m, 7H), 7.34−7.28 (rotamers, m, 3H), 4.30−4.23 (m, 2H), 4.19−4.05 (rotamers, m, 2H), 3.92 (s, 1H), 3.49−3.41 (m, 4H), 3.24−3.16 (m, 2H), 1.68−1.59 (m, 4H), 1.41−1.34 (m, 2H) ppm. Two proton signals are masked by residual water from $CD_3CN$. MS ($ESI^+$): $m/z$ 525.0 $[M]^{2+}$. HR-ESI mass spectrum (acetonitrile:methanol 1:4): found 525.1543; calcd. for $[C_{55}H_{52}N_{10}O_6Ru]/z$ 525.1557.

*$[Ru(phen)_2(Cpp\text{-}L\text{-}PNA\text{-}OH)](PF_6)_2\cdot 3H_2O$ (**M2**).* Complex **M2** was prepared using a similar procedure to that described for **M1** but using **Cpp-L-PNA** (**4**) (0.277 g, 0.4 mmol), $Ru(phen)_2Cl_2$ (0.171 g, 0.32 mmol), and ethanol/$H_2O$ (1:1, 10 mL). The desired monomer **M2** was isolated as a dark orange solid. Yield: 0.360 g (80%). Anal. Calcd. for $C_{59}H_{58}F_{12}N_{10}O_9P_2Ru$ (%): C, 49.14; H, 4.05; N, 9.71. Found: C, 49.22; H, 3.86; N, 9.88. IR (KBr): $\nu$ 3425br (O−H), 3075w (C−$H_{arom}$), 2930m (C−$H_{aliph}$), 2858m (C−$H_{aliph}$), 1690m (C═O), 1658m (C═O), 1650m (C═O), 1531br, 1424br, 1247w, 1225w, 1188w, 1147m, 1088w, 1051w, 1020w, 946w, 840vs, 762m, 742m, 721m $cm^{-1}$. $^1H$ NMR (400 MHz, $CD_3CN$): $\delta$ 9.14−9.11 (m, 1H), 8.66−8.64 (maj) and 8.63−8.61 (min) (rotamers, m, 2H), 8.58−8.54 (m, 2H), 8.40−8.38 (m, 1H), 8.27−8.22 (rotamers, m, 5H), 8.12−8.02 (rotamers, m, 2H), 7.89−7.87 (m, 2H), 7.83−7.76 (m, 5H), 7.69−7.67 (m, 1H), 7.60−7.54 (m, 4H), 7.45−7.40 (rotamers, m, 2H), 7.38−7.35 (m, 2H), 7.33−7.26 (m, 3H), 4.28−4.16 (m, 3H), 4.09−4.06 (min) and 3.91−3.88 (maj) (rotamers, m, 2H), 3.43−3.40 (m, 4H), 3.24−3.15 (rotamers, m, 2H), 1.63−1.57 (m, 4H), 1.39−1.36 (m, 2H) ppm. Two proton signals are masked by residual water from $CD_3CN$. MS ($ESI^+$): $m/z$ 549.1 $[M]^{2+}$. HR-ESI mass spectrum (acetonitrile:methanol 1:4): found 549.1553; calcd. for $[C_{59}H_{52}N_{10}O_6Ru]/z$ 549.1557.

*$[Ru(dppz)_2(Cpp\text{-}L\text{-}PNA)](PF_6)_2$ (**7**).* A solution of *O*-benzotriazole-*N*,*N*,*N*′*N*′-tetramethyl-uronium-hexafluoro-phosphate (HBTU) (0.060 g, 0.158 mmol), 4-dimethylaminopyridine (DMAP) (0.005 g, 0.040 mmol) and $[Ru(dppz)_2(Cpp\text{-}L\text{-}OH)](PF_6)_2$ (**6**) (0.125 g, 0.099 mmol) in dry acetonitrile (4 mL) was stirred for 30 min at room temperature under $N_2$ atmosphere. *tert*-butyl-*N*-[2-(*N*-9-fluorenylmethoxycarbonyl)-aminoethyl]-glycinate·HCl (0.069 g, 0.158 mmol) was added, and the solution stirred for a further 15 min at room temperature. The solution was cooled to 0 °C and *N*,*N*-diisopropylethylamine (DIPEA)


dx.doi.org/10.1021/ic202761w | *Inorg. Chem.* 2012, 51, 3302−3315

(0.028 mL, 0.158 mmol) was added dropwise at the same temperature. The reaction mixture was stirred at 0 °C for a further 30 min before being stirred at room temperature overnight. Acetonitrile was removed under vacuum and water (5 mL) was added to the residue. This resulted in the formation of an orange precipitate which was filtered, washed with water/ether, and air-dried before being washed thoroughly with ethyl acetate to remove unreacted PNA backbone and other organic impurities. The absence of organic impurities in the complex was confirmed by thin layer chromatography (TLC) (silica gel absorbent; 10% methanol/dichloromethane). The orange solid obtained after the ethyl acetate wash was further washed with ether and dried in vacuo to afford **7** as orange solid. Yield: 0.133 g (82%) Anal. Calcd. for $C_{75}H_{64}F_{12}N_{14}O_6P_2Ru$ (%): C, 54.65; H, 3.91; N, 11.90. Found: C, 54.78; H, 3.86; N, 11.79. IR (KBr): $\nu$ 3076w ($CH_{arom}$), 2929m (C−$H_{aliph}$), 2852m (C−$H_{aliph}$), 1683m (C═O), 1654s (C═O), 1649s (C═O), 1548w, 1527m, 1419m, 1409m, 1357m, 1340w, 1236m, 1156s, 1117m, 1080m, 1049w, 954w, 843vs, 762s, 741m, 728s $cm^{-1}$. $^1H$ NMR (400 MHz, DMSO-$d_6$): $\delta$ 9.69−9.63 (m, 1H), 9.60−9.57 (m, 2H), 9.42 (d, $^3J$ = 8.4 Hz, 1H), 8.67−8.65 (m, 1H), 8.49−8.41 (m, 4H), 8.34−8.26 (rotamers, m, 2H), 8.18−8.03 (m, 7H), 7.89−7.81 (m, 8H), 7.66−7.51 (m, 4H), 7.38−7.33 (m, 2H), 7.30−7.28 (m, 2H), 7.24−7.13 (rotamers, m, 2H), 4.34−4.31 (m, 2H), 4.254.18 (m, 3H), 4.02−3.98 (m, 4H), 2.43−2.18 (rotamers, m, 2H), 1.67−1.65 (m, 4H), 1.46 (min) and 1.45 (maj) (s, 9H), 1.44−1.41 (m, 2H) ppm. Two proton signals are masked by residual water in DMSO-$d_6$. MS (ESI$^+$): $m/z$ 679.2 $[M]^{2+}$. HR-ESI mass spectrum (acetonitrile:methanol 1:4): found 679.2065; calcd. for $[C_{75}H_{64}N_{14}O_6Ru]/z$ 679.2088.

*[Ru(dppz)$_2$(Cpp-L-PNA-OH)](PF$_6$)$_2$·6H$_2$O (**M3**).* [Ru(dppz)$_2$(Cpp-L-PNA)](PF$_6$)$_2$ (**7**) (0.252 g, 0.153 mmol) was dissolved in 8 mL solution of dichloromethane/TFA/triethylsilane (55:35:10), which was deoxygenated prior to use. The resulting orange solution was stirred at room temperature for 5 h. Volatiles were removed by rotary evaporation under reduced pressure, and the residue was triturated with toluene (5 × 5 mL) to remove excess TFA. The resulting residue was dissolved in water (5 mL), and an aqueous $HPF_6$ solution (60%) added dropwise to precipitate the product. The precipitate was collected by filtration and purified by column chromatography on silica (acetonitrile/$H_2O$/sat. $KNO_3$ 16:3:1) to collect the dark orange band. The solvent was removed by rotary evaporation, and the residue resuspended in acetonitrile and filtered to remove insoluble $KNO_3$ salt. After removal of solvent, the product was dissolved in water and reprecipitated by dropwise addition of $HPF_6$ (60%). The product was filtered, washed with ether, and dried under high vacuum to give **M3** as an orange powder. Yield: 0.226 g (93%). Anal. Calcd. for $C_{71}H_{68}F_{12}N_{14}O_{12}P_2Ru$ (%): C, 50.15; H, 4.03; N, 11.53. Found: C, 50.02; H, 3.86; N, 11.38. IR (KBr): $\nu$ 3450br (O−H), 3012w ($CH_{arom}$), 2924m (C−$H_{aliph}$), 2851m (C−$H_{aliph}$), 1687m (C═O), 1650s (C═O), 1648s (C═O), 1544w, 1525w, 1442m, 1427m, 1404w, 1352w, 1232w, 1184w, 1135m, 1118m, 1080m, 1052m, 1020w, 844vs, 760s, 743m, 727s $cm^{-1}$. $^1H$ NMR (400 MHz, DMSO-$d_6$): $\delta$ 9.71−9.66 (m, 1H), 9.62−9.59 (m, 2H), 9.44 (d, $^3J$ = 8.4 Hz, 1H), 8.67−8.65 (m, 1H), 8.52−8.47 (m, 3H), 8.39 (d, $^3J$ = 6.0 Hz, 1H), 8.32−8.23 (rotamers, m, 2H), 8.20−8.17 (m, 4H), 8.13−7.97 (rotamers, m, 3H), 7.94−7.81 (m, 8H), 7.63−7.53 (rotamers, m, 4H), 7.37−7.34 (m, 2H), 7.30−7.18 (rotamers, m, 4H), 4.31−4.25 (m, 3H), 4.214.14 (m, 2H), 3.93−3.89 (m, 4H), 2.33−2.12 (rotamers, m, 2H), 1.59−1.52 (m, 4H), 1.36−1.32 (m, 2H) ppm. Two proton signals are masked by residual water from DMSO-$d_6$. MS (ESI$^+$): $m/z$ 651.1 $[M]^{2+}$. HR-ESI mass spectrum (acetonitrile:methanol 1:4): found 651.1777; calcd. for $[C_{71}H_{56}N_{14}O_6Ru]/z$ 651.1777.

**Synthesis of PNA Oligomers.** The SPPS of PNA oligomers was performed following the procedure previously reported by Metzler-Nolte, Gasser, and co-workers.[28,29,53−55] Specifically, the synthesis was manually carried out in one-way polypropylene syringes (5 mL) equipped with a frit, using polystyrene resin beads of TentaGel S RAM Lys(Boc)Fmoc (98 mg, 0.23 mmol/g). The resin was swollen in *N*,*N*′-dimethylformamide for 1 h before use. All reactions were performed at 400 rpm on a mechanical shaker, soaking approximately 3−4 mL of freshly prepared solutions into the syringe. Prior to each coupling step, Fmoc/Bhoc protected PNA monomers (5 equiv) (Link Technologies, Lanarkshire, Scotland) were preactivated in eppendorf tubes for 2 min with HATU (4.5 equiv) in *N*,*N*′-dimethylformamide, adding DIPEA and 2,6-lutidine (10 equiv each) (A(bhoc)-PNA-monomer: 5 min, C(bhoc)-PNA-monomer: 7 min). For each coupling step, the resin beads were treated with the activated acid under vibration and subsequently washed with *N*,*N*′-dimethylformamide. Coupling was monitored with the Kaiser test. Double Fmoc deprotection was performed with piperidine (20%, v/v) in DMF (2 min +10 min). The resin beads were then washed successively with *N*,*N*′-dimethylformamide, dichloromethane, and *N*,*N*′-dimethylformamide. The whole procedure (deprotection, coupling, monitoring) was repeated for every PNA monomer until the PNA sequence was completed.

*Synthesis of Ru-PNA Oligomer (PNA2 (PNA-M1-lys)).* The SPPS of **Ru-PNA** oligomer was performed with slight modification to the general procedure outlined for the synthesis of PNA oligomers. Ru(II)-PNA monomer **M1** (5 equiv) was preactivated in an eppendorf tube before the coupling step for 2 min with HATU (4.5 equiv) in *N*,*N*′-dimethylformamide and adding DIPEA and 2,6-lutidine (10 equiv each). A longer reaction time of 10 h was allowed to ensure a full coupling. Subsequent coupling steps were performed as described before, allowing each reaction to continue for 2.5 h until the PNA sequence was completed.

*Synthesis of Ru-PNA-NLS Oligomer (PNA3 (NLS-PNA-M1-lys)).* *N*-terminus solid-phase insertion of the amino acids on the Ru-PNA oligomer was achieved by following the general SPPS procedure. Amino acid coupling followed the Fmoc deprotection of the last PNA monomer of the respective PNA sequence. The amino acids (Fmoc-L-Val-OH/Fmoc-L-Lys(Boc)-OH/Fmoc-L-Pro-OH.$H_2O$/Fmoc-L-Arg-(Pbf)-OH) (5 equiv) were preactivated in eppendorf tube with HOBt and TBTU (4.5 equiv each) in *N*,*N*′-dimethylformamide and adding DIPEA and 2,6-lutidine (10 equiv each). Double coupling was applied to ensure full conversion.

*Cleavage of the PNA from the Resin.* Before cleavage, the resin containing the PNA was contracted with methanol and dried. The nonmetal-containing PNAs were cleaved using a mixture of TFA:water:triisopropylsilane 95:2.5:2.5 while the metallic-containing PNAs were cleaved using a mixture of TFA:triisopropylsilane:phenol 85:5:10 [3 × 400 $\mu$L (1.5 h each)]. The TFA was removed from the resulting solutions under high vacuum before the crude oligomers being precipitated with ice-cold ether. The solids were centrifuged, washed with ice-cold ether, and finally air-dried. The crude oligomers were purified with RP-HPLC, as described under Instrumentation and Methods, and characterized by ESI-MS and MALDI-TOF mass spectrometry.

*Characterization of PNA1.* ESI-MS: $m/z$ 373.1 $[M+7H]^{7+}$, 435.3 $[M+6H]^{6+}$, 522.1 $[M+5H]^{5+}$, 652.3 $[M+4H]^{4+}$, 869.5 $[M+3H]^{3+}$, 1304.0 $[M+2H]^{2+}$. MALDI-TOF: $m/z$ 2605.8 $[M+H]^+$.

*Characterization of PNA2 (PNA-M1-lys).* ESI-MS: $m/z$ 427.7 $[M+8H]^{8+}$, 488.7 $[M+7H]^{7+}$, 570.0 $[M+6H]^{6+}$, 683.8 $[M+5H]^{5+}$, 854.4 $[M+4H]^{4+}$. MALDI-TOF: $m/z$ 3415.5 $[M+H]^+$.

*Characterization of PNA3 (NLS-PNA-M1-lys).* ESI-MS: $m/z$ 428.8 $[M+10H]^{10+}$, 476.4 $[M+9H]^{9+}$, 535.9 $[M+8H]^{8+}$, 612.3 $[M+7H]^{7+}$, 714.1 $[M+6H]^{6+}$. MALDI-TOF: $m/z$ 4279.7 $[M+H]^+$.

*Characterization of PNA4 (NLS-PNA-lys).* ESI-MS: $m/z$ 434.8 $[M+8H]^{8+}$, 496.8 $[M+7H]^{7+}$, 579.4 $[M+6H]^{6+}$, 695.1 $[M+5H]^{5+}$, 868.6 $[M+4H]^{4+}$. MALDI-TOF: $m/z$ 3470.3 $[M+H]^+$.

**PNA and DNA Concentration Determination.** PNA stock solutions were prepared in nanopure water and stored at −18 °C. The strand concentration of PNA/DNA oligomers was estimated by UV spectroscopy at 80 °C using the sum of molar extinction coefficients at 260 nm ($\varepsilon_{260}$) for PNA and DNA nucleobases present in the oligomeric strands ($\varepsilon_{DNA,A}$ = 15300 $M^{-1}$ $cm^{-1}$, $\varepsilon_{DNA,G}$ = 12200 $M^{-1}$ $cm^{-1}$, $\varepsilon_{DNA,C}$ = 7600 $M^{-1}$ $cm^{-1}$, $\varepsilon_{DNA,T}$ = 8700 $M^{-1}$ $cm^{-1}$, $\varepsilon_{PNA,A}$ = 13700 $M^{-1}$ $cm^{-1}$, $\varepsilon_{PNA,G}$ = 11700 $M^{-1}$ $cm^{-1}$, $\varepsilon_{PNA,C}$ = 6600 $M^{-1}$ $cm^{-1}$, $\varepsilon_{DNA,T}$ = 8600 $M^1cm^1$).[2] Because of the limited solubility of monomer **M1** in aqueous solution, the molar extinction coefficient of the Ru(II) complex at 260 nm, $\varepsilon_{260}$ = 13300 $M^{-1}$ $cm^{-1}$ was estimated using $[Ru(bpy)_3]^{2+}$ as model compound. It was determined from the slope of the absorption ($A_{260}$) versus concentration curve.


dx.doi.org/10.1021/ic202761w | *Inorg. Chem.* 2012, 51, 3302−3315

**Scheme 1. Synthesis of Racemic Mixtures of M1 and M2**

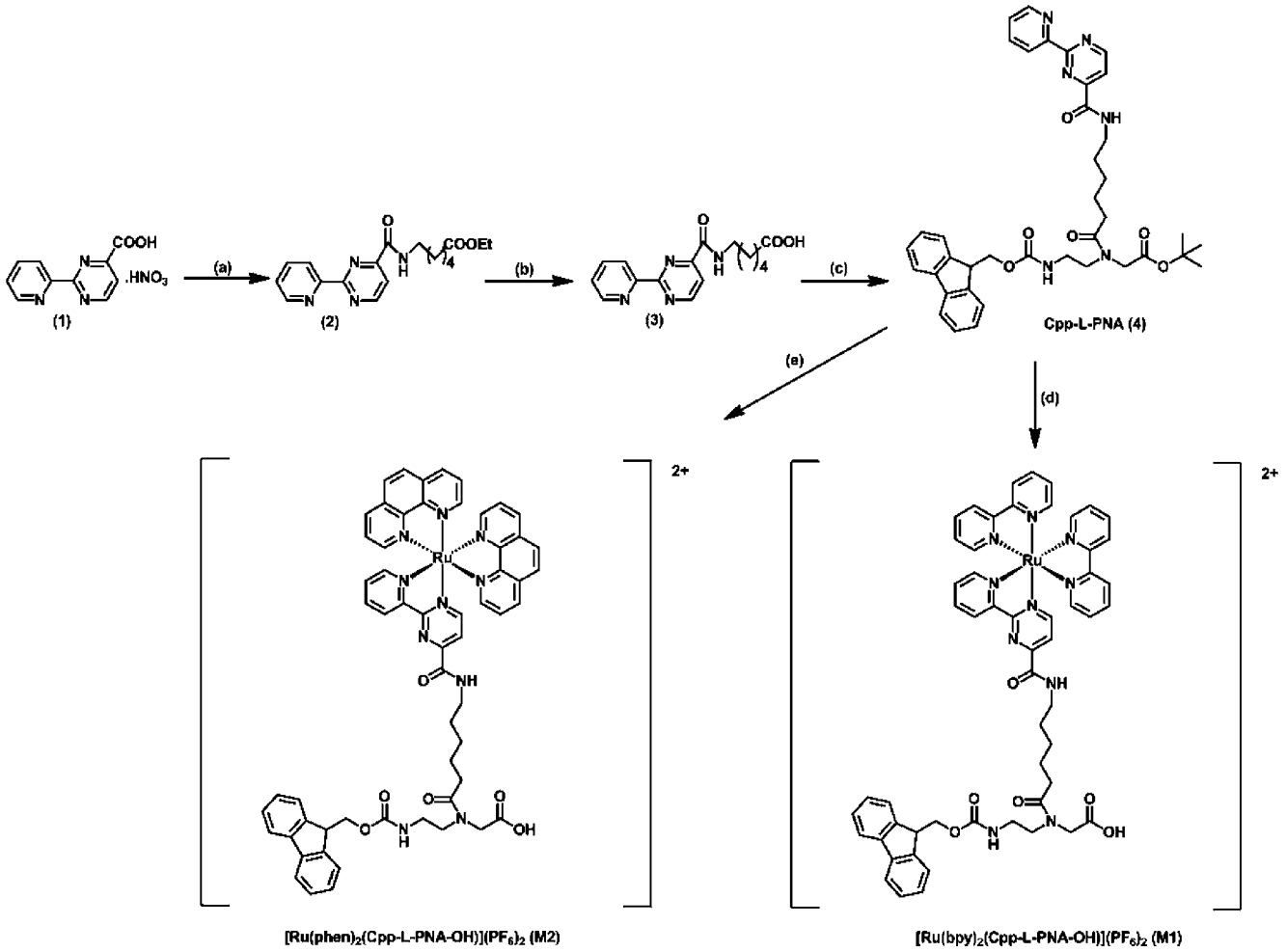


Reagents and conditions: (**a**) ethyl 6-aminohexanoate hydrochloride, HOBt, DCC, DMAP, $Et_3N$, dry acetonitrile, rt, 16 h, 79%; (**b**) NaOH, methanol/$H_2O$ (3:1), 0 °C-rt, 16 h, 87%; (**c**) *tert*-butyl *N*-[2-(*N*-9-fluorenylmethoxycarbonyl)aminoethyl]glycinate, HBTU, $Et_3N$, dry *N*,*N*′-dimethylformamide, DIPEA, rt, 18 h, 82%; (**d**) 1. TFA/dichloromethane (1:1), rt, 4 h; 2. $Ru(bpy)_2Cl_2$, ethanol/$H_2O$ (1:1), Δ, 5 h, 85%; (**e**) 1. TFA/dichloromethane (1:1), rt, 4 h; 2. $Ru(phen)_2Cl_2$, ethanol/$H_2O$ (1:1), Δ, 5 h, 80%.

**Thermal Melting Curves.** UV melting experiments were carried out on equimolar mixtures of PNA and DNA concentrations consisting of 3 μM of each in 10 mM PBS buffer (pH 7.4) solution. Samples were annealed by heating at 90 °C for 20 min before cooling to 20 °C over 2 h. Thermal program: starting and returning temperature = 25 °C; heating to 90 °C, cooling to 4 °C, each at 0.5 °C/min and holding for 3 min at the end-temperatures with data points collected every 0.2 °C; absorbance was monitored at 260 nm. The $T_m$ values, obtained as the maxima of the first derivative plots of $A_{260}$ versus $T$, were an average of four separate experiments ± standard deviation.

**Circular Dichroism (CD) Experiments.** CD spectra were measured for annealed 3 μM solutions of **PNA·DNA** duplexes in pH 7.4 sodium phosphate buffer (10 mM). All spectra were recorded at room temperature between 200 and 350 nm using a scan speed 200 nm/min; response time 1.0 s; bandwidth 1.0 nm; scan accumulations 10; and were corrected for the buffer background.

## RESULTS AND DISCUSSION

**Synthesis of Ru(II)-PNA-like Monomers.** The PNA-like monomers, $[Ru(bpy)_2(Cpp\text{-}L\text{-}PNA\text{-}OH)](PF_6)_2$ (**M1**), $[Ru(phen)_2(CppL\text{-}PNA\text{-}OH)](PF_6)_2$ (**M2**), and $[Ru(dppz)_2(Cpp\text{-}L\text{-}PNA\text{-}OH)](PF_6)_2$ (**M3**), were prepared as described in Schemes 1 and 2. The 4′-methyl-2,2′-bipyridine (Mebpy) ligand backbone which had been used for previously reported Ru(II)-polypyridyl PNA monomers[44] was replaced by 2-(2′-pyridyl)-pyrimidine-4-carboxylic acid (CppH) ligand (**1**, Scheme 1). This was done to avoid synthetic difficulties without significantly altering the photophysical and electrochemical properties of the envisioned products.[49] An alkyl spacer was introduced between the metal coordinating CppH unit and the PNA backbone,[56] to minimize the steric interference from the Ru(II) subunit in the hydrogen bonding between the PNA-DNA. Following trifluoroacetic acid mediated in situ deprotection of the *tert*-butyl group in the PNA-like monomeric template unit, **Cpp-L-PNA** (**4**), the free carboxylic acid derivative was reacted with $Ru(bpy)_2Cl_2$ or $Ru(phen)_2Cl_2$ under inert atmosphere. This afforded **M1** and **M2** in about 80% yield which were isolated as their $PF_6^-$ salts. Complex reaction mixtures were obtained for a similar reaction between $Ru(dppz)_2Cl_2$ and **Cpp-L-PNA**. The need to use harsh chemical conditions and high reaction temperatures led to an alternative synthesis for the dipyrido[3,2-*a*:2′,3′-*c*]phenazine (dppz) based PNA-like monomer, **M3** (Scheme 2). This involved the chemical decarbonylation of $[Ru(CO)_2Cl_2]_n$ and the intermediate complex (**5**)[49] to prepare $[Ru(dppz)_2(Cpp\text{-}L\text{-}OH)](PF_6)_2$, (**6**).


dx.doi.org/10.1021/ic202761w | *Inorg. Chem.* 2012, 51, 3302−3315

**Scheme 2. Synthetic Route for Preparation of M3 (Racemic Mixture)**

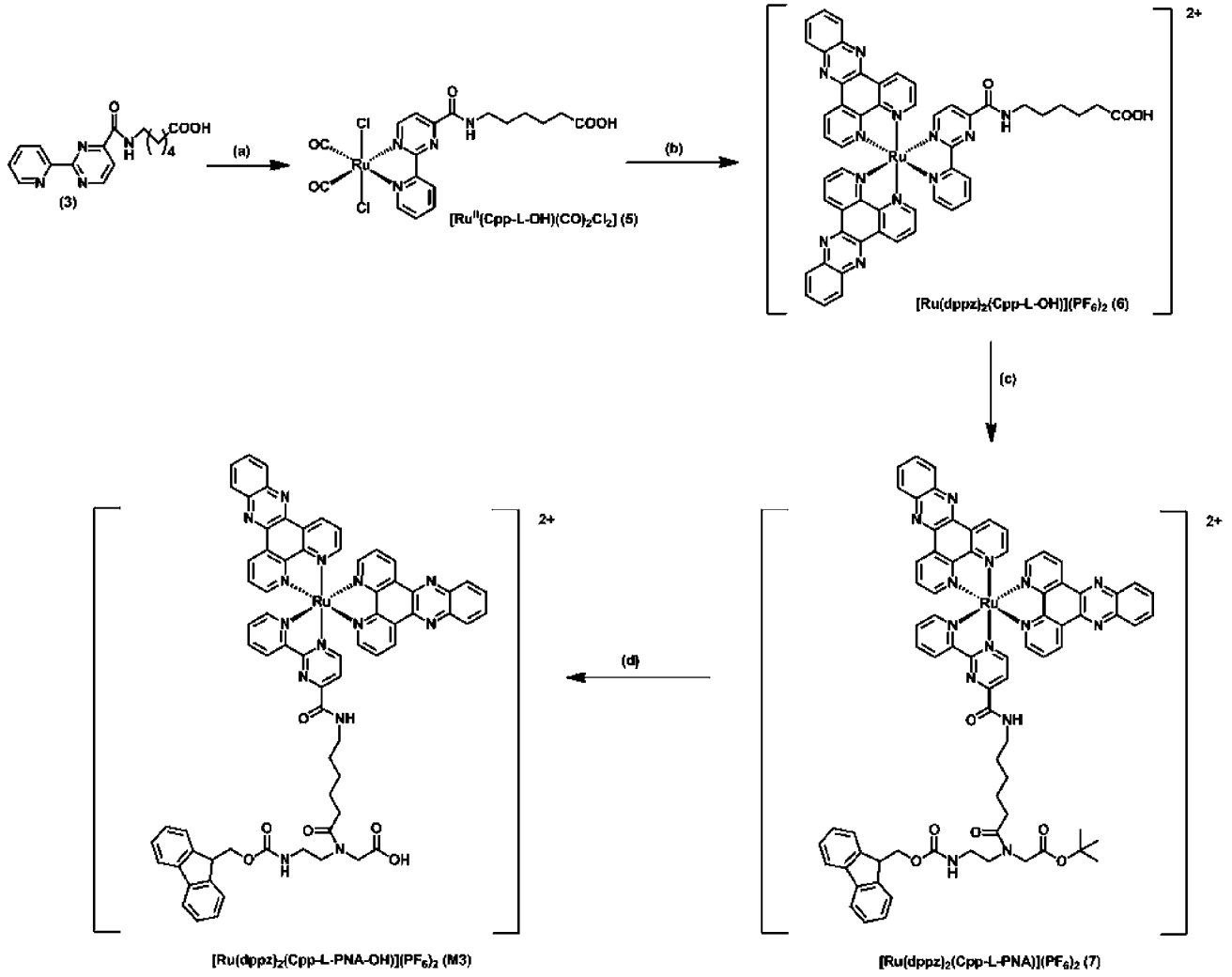


Reagents and conditions: (a) $[Ru(CO)_2Cl_2]_n$, methanol, Δ, 2 h, 85%; (b) 1. dppz, $Me_3NO$, 2-methoxyethanol, Δ, 4 h; 2. acetonitrile/$H_2O$/$H_2SO_4$ (45:45:10), Δ, 24 h, 68%; (c) *tert*-butyl *N*-[2-(*N*-9-fluorenylmethoxycarbonyl)amino ethyl]glycinate, HBTU, $Et_3N$, dry acetonitrile, DIPEA, rt, o/n, 82%; (d) dichloromethane/TFA/triethylsilane (55:35:10), rt, 5 h, 93%.

Subsequent attachment on the PNA backbone followed by TFA mediated deprotection of the *tert*-butyl group afforded **M3** in 93% yield. The identity of **M1**, **M2**, and **M3** was confirmed by ESI-MS (*m*/*z* 525.0, 549.1 and 651.1, respectively, for $[M]^{2+}$), $^1$H NMR spectroscopy, IR spectroscopy, and elemental analysis. In the IR spectrum, aliphatic and aromatic C−H stretches were observed between 2850 and 3080 $cm^{-1}$ and carbonyl stretches in the 1650−1690 $cm^{-1}$ region, which were assigned to amide and ester functionalities. Additional aromatic signals for the introduced bipyridine, phenanthroline, or dipyridophenazine ligands and the disappearance of *tert*-butyl $CH_3$ signal (ca. 1.45 ppm) in the $^1$H NMR spectrum further verified the successful isolation of the Ru(II)-PNA-like monomers.

**Ru(II)-PNA Oligomer Synthesis.** Chemical feasibility for solid support incorporation of the Ru(II) PNA-like monomers within a PNA sequence was demonstrated by manual Fmoc based solid phase PNA synthesis on Fmoc-Lys(Boc) preloaded TentaGel S RAM resin (Scheme 3). The choice of the PNA sequence was determined with a view to biological testing to be undertaken in the future. The monomer **M1** was successfully introduced within the PNA oligomers (see Table 1) by coupling it to the Fmoc-deprotected lysine residue available on the resin. Long reaction times were allowed to ensure efficient coupling of **M1** before proceeding with the synthesis of the remaining 9-mer PNA sequence (**PNA1**) or NLS-PNA (**PNA4**), respectively. Cleavage from the resin with TFA/TIS/phenol 85:5:10 (v/v/v), precipitation with diethyl ether followed by centrifugation gave the Ru-PNA oligomers, **PNA2** (PNA-***M1***-lys) and **PNA3** (NLS-PNA-***M1***-lys), in good yield and purity as confirmed by LC-MS and MALDI-TOF MS (see the Supporting Information, Figures S4−S11). The successful isolation of **PNA2** and **PNA3** demonstrates the chemical stability of the Ru(II)-subunits in **PNA2** and **PNA3** under solid phase synthesis conditions and exemplifies the benefit of using the modified monomers for preparing the metal-PNA bioconjugates.[7] As shown for **PNA3**, the *N*-terminus of the Ru(II)-labeled PNA oligomers can be used to further attach the peptide moieties (NLS peptide sequence PKKKRKV in this case)[57] prior to their cleavage from the solid support. This strategy can be conveniently adapted for the preparation of Ru(II)-PNA oligomers with enhanced solubility and cellular uptake properties suitable for effective in vivo applications. Besides this, efforts were also made to incorporate the PNA-like monomer


dx.doi.org/10.1021/ic202761w | *Inorg. Chem.* 2012, 51, 3302−3315

**Scheme 3. General Procedure for Solid Phase Synthesis of PNA-Ru(II) Conjugates**

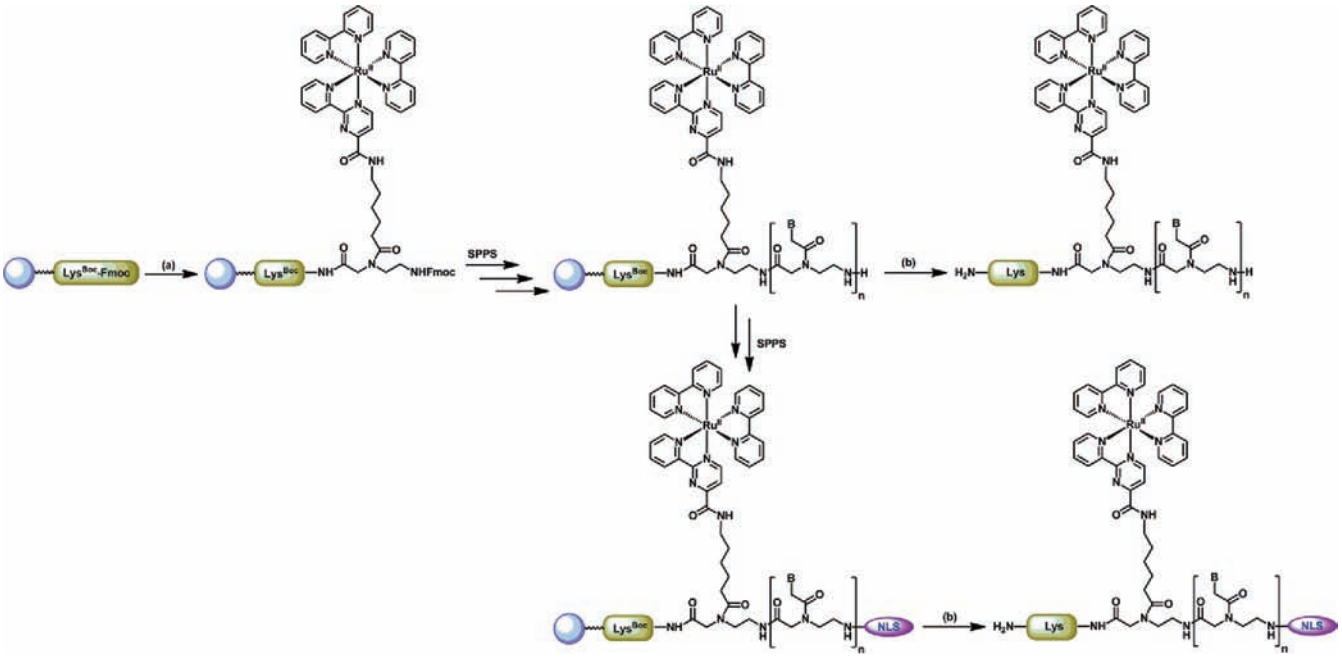


Reagents and conditions: (**a**) $[Ru(bpy)_2(Cpp\text{-}L\text{-}PNA\text{-}OH)](PF_6)_2$, HATU, *N*,*N*′-dimethylformamide, 10 h; (**b**) TFA/TIS/Phenol (85:5:10). SPPS = Standard Fmoc solid phase PNA/peptide synthesis. See Experimental Section for details.

**Table 1. PNA Sequences Prepared As Part of This Study**[a]

| PNA code | sequence[b] | $[M+H]^+$ (found)[c] | $[M+H]^+$ (calcd.) |
|---|---|---|---|
| **PNA1** | H-g-c-a-a-t-a-a-a-a-lys-$NH_2$ | 2605.8 | 2605.1 |
| **PNA2** | H-g-c-a-a-t-a-a-a-a-***M1***-lys-$NH_2$ | 3415.5 | 3415.3 |
| **PNA3** | H-P-K-K-K-R-K-V-g-c-a-a-t-a-a-a-a-***M1***-lys-$NH_2$ | 4279.7 | 4279.9 |
| **PNA4** | H-P-K-K-K-R-K-V-g-c-a-a-t-a-a-a-a-lys-$NH_2$ | 3470.3 | 3469.7 |

[a]Small letters a, t, g, c denote PNA monomers while the amino acids are represented using standard 1 letter codes. PNA sequences are written from *N*- to *C*- terminus. [b]Manual Fmoc based solid-phase synthesis. [c]Measured by MALDI-TOF MS.

**M3** within the oligomeric sequence. However, the coupling could not be achieved despite attempting several alterations to the synthetic strategy. This included noncovalent premodification of the resin with sulforhodamine to increase the availability of **M3** during the coupling step. Corey et al.[58] applied this method to improve the efficiency of solid phase coupling in the case of fluorophores. Overall, these outcomes collectively demonstrate that the assembly of the PNA oligomers on the solid support, and its subsequent cleavage, is not entirely unaffected by the presence of such Ru(II) PNA-like monomers within the sequence. Nevertheless, it is feasible if monomers are suitably designed to avoid any spatial steric constraints for coupling to occur.

**UV−vis Absorption Spectroscopy of Ru(II)-PNA-like Monomers.** The UV−visible spectrum of **M1**−**M3** measured in acetonitrile displayed bands for ligand centered (LC) and metal to ligand charge transfer (MLCT) transitions, as shown in Table 2 and Figure 2. The absorption bands between 250 and 300 nm were assigned to the LC transitions, and the broad band centered around 450 nm to a MLCT transition between the 4d metal orbital and $\pi^*$ ligand orbitals. An additional band at 363 nm for the intraligand charge transfer in the dppz unit

**Table 2. UV-Vis Spectral Data Obtained for 10 $\mu$M Acetonitrile Solutions of M1−M3**

| Complex | $\lambda_{max}$ (nm) [LC] | $\varepsilon_{max}$ ($M^{-1}$ $cm^{-1}$) | $\lambda_{max}$ (nm) [MLCT] | $\varepsilon_{max}$ ($M^{-1}$ $cm^{-1}$) |
|---|---|---|---|---|
| **M1** | 252 | 29400 | 448 | 10300 |
| | 283 | 55400 | | |
| **M2** | 263 | 88500 | 443 | 14400 |
| **M3** | 278 | 74600 | 449 | 10900 |
| | 363 | 18100 | | |

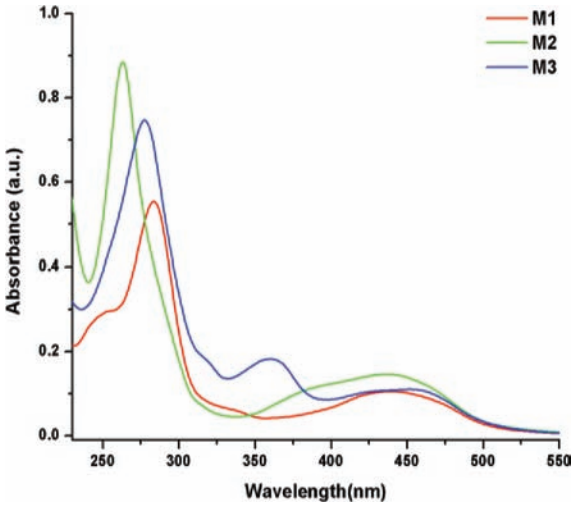


**Figure 2.** Absorption spectra of Ru(II)-PNA monomers **M1**−**M3** (10 $\mu$M) in acetonitrile.

was also observed. The UV−visible transitions for the PNA monomers are consistent with those reported for other Ru(II)-polypyridyl complexes.[31,33,44,45,49] The transitions overlapped with those observed for the respective carboxylic acid


dx.doi.org/10.1021/ic202761w | *Inorg. Chem.* 2012, 51, 3302−3315

precursors, $[Ru(bpy)_2(CppH)](PF_6)_2$[49] and $[Ru(bpy)_2(Cpp\text{-}L\text{-}OH)](PF_6)_2$ for **M1**, and $[Ru(dppz)_2(CppH)](PF_6)_2$ and $[Ru(dppz)_2(Cpp\text{-}L\text{-}OH)](PF_6)_2$ for **M2**. As expected, modifications made to the pyridyl-pyrimidine ligand backbone had little effect on the $^1$MLCT transitions.

**Photoluminescence Spectroscopy of Ru(II)-PNA-like Monomers.** Emission spectral data for complexes, **M1**−**M3**, measured following excitation of 10 $\mu$M complex solutions at 450 nm are summarized in Table 3 (Supporting Information, Figure S12 illustrates the respective emission profiles). The emission maxima were found to be red-shifted compared to $[Ru(bpy)_3]^{2+}$ (615 nm); 665, 651, and 637 nm for **M1**, **M2**, and **M3**, respectively. On the basis of literature precedence, the observed luminescence is attributed to the decay of the triplet excited state ($^3$MLCT).[31,49] For **M1** and **M3**, the emission maxima were red-shifted relative to the parent CppH complexes, $[Ru(bpy)_2(CppH)]^{2+}$ and $[Ru(dppz)_2(CppH)]^{2+}$ (Table 3). This red shift along with the overlap of their maxima with those of the respective carboxylic acid precursors, $[Ru(bpy)_2(Cpp\text{-}L\text{-}OH)]^{2+}$ and $[Ru(dppz)_2(Cpp\text{-}L\text{-}OH)]^{2+}$, suggest no major influence from the attached PNA backbone. Instead, minor energetic differences most likely arise from the conversion of the carboxylic acid group on the pyridyl-pyrimidine ring into an amide. The emission intensities, expressed as number of photons between 500 and 800 nm, followed the trend as **M3** > **M2** > **M1**. The emission intensities for **M1** and **M3** were lower than for their respective parent complexes, $[Ru(bpy)_2(CppH)]^{2+}$ and $[Ru(dppz)_2(CppH)]^{2+}$. Quantum yields for emission from **M1**−**M3** were estimated from the extinction coefficient for absorption at 450 nm and the respective integrated emission intensities as:

$$\Phi_R = \Phi_{ref}(I_s A_{ref})/(I_{ref} A_s)$$

where, $I_s$ and $I_{ref}$ refer to the integrated emission intensity calculated from the area under the emission spectrum of the sample and reference, respectively, and $A_s$ and $A_{ref}$ refer to the absorbance of the sample and reference from the UV−vis spectra, respectively.[33,44,49] The quantum yield ($\Phi_{ref}$) for $[Ru(bpy)_3]^{2+}$ was taken as 0.062 in acetonitrile.[33] The quantum yields followed the same trend as the emission intensities with the bis(dppz) based Ru(II)-PNA-like monomer, **M3**, displaying highest quantum yield. The higher quantum yield values for **M3** relative to **M1** and **M2** indicates that the ancillary dppz ligands may be influencing the $^3$MLCT excited state. This state is also affected by the changes in the functional group (carboxylic acid vs amide linkage) attached to pyridyl-pyrimidine ligand.

**Table 3. Summary of Data Obtained from Emission Spectra of Ru(II) Complexes[a] Following Excitation at 450 nm**

| complex[b] | $\lambda_{max}$ (nm) | $I_s/I_{ref}$ | $\Phi_R$ |
|---|---|---|---|
| **M1** | 665 | 0.69 | 0.052 |
| **M2** | 651 | 0.95 | 0.052 |
| **M3** | 637 | 1.32 | 0.092 |
| $[Ru(bpy)_2(CppH)]^{2+}$ | 623 | 0.85 | 0.048 |
| $[Ru(bpy)_2(Cpp\text{-}L\text{-}OH)]^{2+}$ | 667 | 0.68 | 0.050 |
| $[Ru(dppz)_2(CppH)]^{2+}$ | 628 | 1.36 | 0.078 |
| $[Ru(dppz)_2(Cpp\text{-}L\text{-}OH)]^{2+}$ | 638 | 1.79 | 0.071 |
| $[Ru(bpy)_3]^{2+}$[c] | 615 | 1.00 | 0.062 |

[a] 10 ± 1 $\mu$M solutions in acetonitrile. [b] Abbreviations: **bpy** = 2,2′-bipyridine, **dppz** = dipyrido[3,2-a:2′,3′-c]phenazine, **CppH** = 2-(pyridin-2-yl)pyrimidine-4-carboxylic acid, **Cpp-L-OH** = 6-(2-(pyridin-2-yl)pyrimidine-4-carboxamido)hexanoic acid. [c] Ref 59.

**Electrochemistry of Ru(II)-PNA-like Monomers.** The electrochemical behavior of **M1**−**M3** was studied by cyclic voltammetry at a 1 mM concentration in acetonitrile solutions containing 0.1 M $nBu_4NPF_6$ as the supporting electrolyte and over a scan rate range of 100−1000 mV s$^{-1}$. Representative cyclic voltammograms and scan rate dependences are displayed in Figure 3 and Supporting Information, Figures S13−S15, respectively. The cyclic voltammetry revealed a reversible one electron $Ru^{II}$ to $Ru^{III}$ oxidation process. The formal reversible potential ($E^\circ_f$) was assumed to be equal to the midpoint potential and, hence, calculated as the average of the respective oxidation ($E_p^{ox}$) and reduction ($E_p^{red}$) peak potentials (Supporting Information, Table S1). The values were 974, 980, and 1067 mV for **M1**, **M2**, and **M3**, respectively (vs $Fc^{0/+}$). They are more positive than that for $[Ru(bpy)_3]^{2+}$ (888 mV vs $Fc^{0/+}$).[49] The systematic increase in $E^\circ_f$ ($Ru^{2+/3+}$) on going from the bis(bipyridyl) to the bis(phenanthroline) to the bis(dipyridophenazine) compounds indicates an increase in electron delocalization arising from the increased aromatic nature. This stabilizes the highest occupied molecular orbital (HOMO) and, hence, increases the formal reversible potential of the complex. This along with a widening of the gap between the HOMO and lowest unoccupied molecular orbital (LUMO) on going from **M1** to **M3**, as deduced from the blue shift in emission maxima (vide supra), prompts us to propose that the LUMO energy levels for **M1**, **M2**, and **M3** are similar. Furthermore, this implies that the LUMO is located on the pyridyl-pyrimidine based ligand (Cpp) in each case. That **M1** is red-shifted compared with $[Ru(bpy)_3]^{2+}$, despite having a higher oxidation potential, further supports the notion of a low lying, Cpp-localized LUMO.

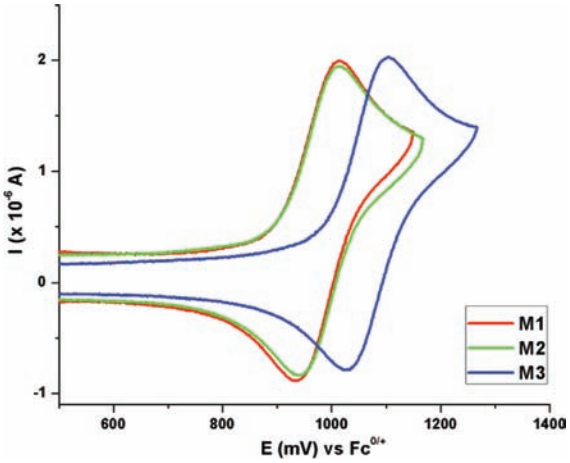


**Figure 3.** Cyclic voltammograms obtained at a glassy carbon electrode using a scan rate of 100 mV s$^{-1}$ for the oxidation of 1 mM Ru(II)-PNA monomers in acetonitrile (0.1 M $nBu_4NPF_6$).

A linear relationship was observed between oxidation peak current ($i_p^{ox}$) and square root of the scan rate ($\nu^{1/2}$), and so the Randles−Sevcik equation[60−62] was used to calculate the diffusion coefficients. The values for **M1**−**M3** were found to be (1.22 ± 0.1) × 10$^{-5}$ cm$^2$ s$^{-1}$, (1.18 ± 0.1) × 10$^{-5}$ cm$^2$ s$^{-1}$, and (1.17 ± 0.1) × 10$^{-5}$ cm$^2$ s$^{-1}$, respectively. These values are similar to those previously reported for other Ru(II) polypyridyl complexes and Ru(II)-PNA monomer derivatives.[44,45] Although the Ru(II) complexes also exhibited a series of complicated ligand-based reduction processes under


dx.doi.org/10.1021/ic202761w | Inorg. Chem. 2012, 51, 3302−3315

voltammetric conditions, the present study is focused only on details relative to the $Ru^{II}$ to $Ru^{III}$ oxidation process.

**ECL Properties of Ru(II)-PNA-like Monomers.** This ECL study of **M1**−**M3** adds to our recent endeavors to create a library of Ru(II)-PNA-like monomers which can be exploited as ECL biosensors.[45] The ECL signal was generated from acetonitrile solutions of 0.1 mM Ru(II) complexes using 0.1 M TPA as co-reactant. Low complex concentrations were chosen for ECL experiments bearing in mind the conditions of practical biosensing applications. ECL profiles are presented in Figure 4, and the data is summarized in Table 4. The ECL emission maxima values for **M1**−**M3** were 665, 655, and 640 nm

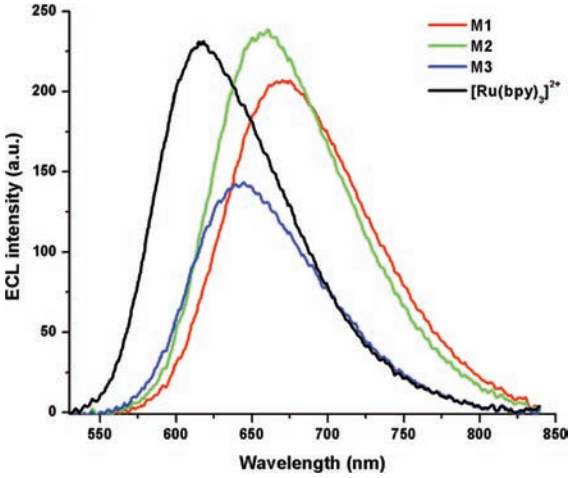


**Figure 4.** ECL emission spectra of **M1**−**M3** and $[Ru(bpy)_3]^{2+}$ complexes (0.1 mM in acetonitrile, 0.1 M TPA).

**Table 4. Summary of ECL Emission Data for Ru(II) Complexes**[a]

| complex[b] | $\lambda_{ECL}$ (nm) | ECL intensity (%)[d] |
|---|---|---|
| **M1** | 667 | 98 |
| **M2** | 655 | 107 |
| **M3** | 640 | 61 |
| $[Ru(bpy)_2(CppH)]^{2+}$ | 661 | 73 |
| $[Ru(bpy)_2(Cpp\text{-}L\text{-}OH)]^{2+}$ | 661 | 55 |
| $[Ru(dppz)_2(CppH)]^{2+}$[c] | 650 | 38 |
| $[Ru(dppz)_2(Cpp\text{-}L\text{-}OH)]^{2+}$ | 659 | 59 |
| $[Ru(bpy)_3]^{2+}$[e] | 618 | 100 |

[a]Conditions: [complex] = 0.1 mM, [TPA] = 0.1 M (acetonitrile, 0.1 M $TBAPF_6$). [b]Abbreviations: **bpy** = 2,2′-bipyridine, **dppz** = dipyrido-[3,2-*a*:2′,3′-*c*]phenazine, **CppH** = 2-(pyridin-2-yl)pyrimidine-4-carboxylic acid, **Cpp-L-OH** = 6-(2-(pyridin-2-yl)pyrimidine-4-carboxamido)-hexanoic acid. [c][complex] = 0.2 mM. [d]Integrated ECL intensity for $[Ru(bpy)_3]^{2+}$ was arbitrarily set as 100%. [e]Ref 45.

respectively, with no ECL signal detected from the metal-free PNA backbone in control experiments.

Co-reactant ECL in Ru(II) complexes occurs as a result of a cascade of electrochemical and chemical reactions involving both the complex and the co-reactant (for example TPA) described as:[45,63−65]

$$[Ru(L)_3]^{2+} \rightleftharpoons [Ru(L)_3]^{3+} + e^- \quad (1)$$

$$N(C_3H_7)_3 \rightleftharpoons N(C_3H_7)_3^{\bullet+} + e^- \quad (2)$$

$$N(C_3H_7)_3^{\bullet+} \rightleftharpoons CH_3CH_2C^{\bullet}HN(C_3H_7)_2 + H^+ \quad (3)$$

$$CH_3CH_2C^{\bullet}HN(C_3H_7)_2 + [Ru(L)_3]^{3+} \rightleftharpoons [Ru(L)_3]^{2+*} + P \quad (4)$$

$$[Ru(L)_3]^{2+*} \rightleftharpoons [Ru(L)_3]^{2+} + h\nu \quad (5)$$

The TPA radical cation product of reaction 2 can be also formed by reaction with the co-existing $[Ru(L)_3]^{3+}$ species.[45,63−65]

For our studies, the integrated emission intensities are compared using the ECL emission from $[Ru(bpy)_3]^{2+}$ as reference (Table 4). The so obtained ECL emission intensity data differ in trend from the photoluminescence data (vide supra). The emission response for **M1**, the PNA monomer with the bis(bpy)-Ru(II) unit, was found to be significantly higher than for the carboxylic acid precursors. However, such a dramatic variation was not observed in ECL generated from **M3**, the monomer with a bis(dppz)Ru(II) unit. The ECL intensity percentage varies as **M2** (107%) ≥ $[Ru(bpy)_3]^{2+}$ (100%) ≥ **M1** (98%) > **M3** (61%) with the monomers **M2** and **M3** displaying intensities at par with the benchmark ECL emitter $[Ru(bpy)_3]^{2+}$. The high ECL intensities for these Ru(II) PNA-like monomers make them potentially strong contenders for use as ECL labels. The reciprocated ECL intensities and photoluminescence efficiency ($\Phi_R$) trends for **M2** and **M3**, when compared to **M1**, can be rationalized on the basis of the higher oxidation potential of **M3**. This increases the possibility of the Ru(III) species taking part in parasitic side reactions which decrease the yield of excited states and reduce the ECL efficiency. Overall, the photoluminescence efficiency and ECL emission intensity data sets reaffirm the complexity of ECL generation in such systems.[33,38,39,45,63−67]

**Spectroscopic Properties of Ru(II)-PNA Oligomers.** The UV−visible spectra for the Ru(II)-PNA oligomers, **PNA2** and **PNA3**, as well as their **PNA·DNA** hybrids were recorded at 3 $\mu$M strand concentrations in PBS buffer (pH 7.4). The cDNA strand (**DNA:** 5′-T-T-T-**T-T-T-T-T**-A-**T-T-G-C**-T-T-T-3′) was extended with three thymine residues on the 3′ and 5′ ends. Duplex formation was induced by heating the equimolar solutions at 90 °C for 10 min followed by slowly cooling to room temperature over a period of 2 h. As shown in Figure 5, the spectra for the Ru(II)-PNA oligomers showed $\pi-\pi^*$ transition bands for the PNA nucleobases as well as the LC transitions from the Ru(II)-polypyridyl unit inserted within the PNA sequence. These transitions dominated the spectral region between 250 and 300 nm whereas MLCT transitions were again centered around 445 nm. Metzler-Nolte and co-workers earlier reported a similar absorption profile for their Ru(II)-PNA conjugates.[68] The position and intensity of the MLCT remained unchanged for the **PNA2·DNA** and **PNA3·DNA** duplexes. The spectra also displayed a broad absorption band centered around 267 nm assigned to $\pi-\pi^*$ transitions in the PNA and DNA nucleobases and the polypyridyl ligands surrounding the Ru(II) center. The emission spectra for the Ru(II)-PNA oligomers, with excitation at 450 nm, exhibited maxima at 688 and 682 nm for **PNA2** and **PNA3**, respectively. Upon hybridization with the cDNA strand, the position of the maxima and emission intensity for **PNA2·DNA** and **PNA3·DNA** duplexes remained unchanged. The absence of large changes in the MLCT and the emission profile of the Ru-**PNA·DNA** duplexes versus their respective single stranded


dx.doi.org/10.1021/ic202761w | *Inorg. Chem.* 2012, 51, 3302−3315

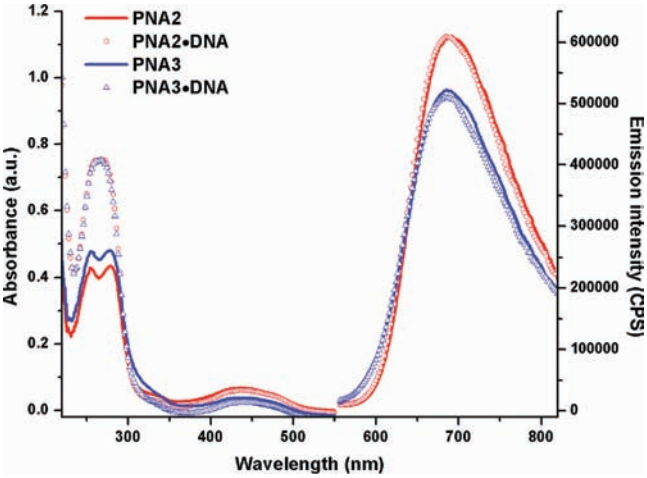


**Figure 5.** Electronic absorption and emission spectra of Ru(II)-PNA sequences and their duplexes with cDNA (3 $\mu$M in 10 mM PBS (pH 7.4) buffer).

sequence indicate that the $^1$MLCT and $^3$MLCT excited states involved in these transitions remain more or less unaffected by the hybridization process. The dangling alkyl linker in the Ru(II)-polypyridyl luminophoric unit could be allowing reorganization within the duplex to accommodate the hydrogen bonding and base stacking interactions.

**ECL Analysis of Ru(II)-PNA Oligomers.** The solution phase ECL response from the Ru(II)-PNA oligomers, **PNA2** and **PNA3**, was studied in 0.1 M PBS (pH 7.4) buffer. In each case, 0.1 $\mu$M Ru(II)-PNA solutions were used in the presence of 0.1 M tripropylamine (TPA) as co-reactant. Once again, high co-reactant levels and small PNA concentrations were chosen to simulate the context in which such Ru(II)-PNA oligomer systems would be used in practical biosensing applications. The cyclic voltammograms for **PNA2** (Figure 6, curve D) showed no distinctive redox peaks for the $Ru^{2+/3+}$ because of the low concentration of the Ru(II)-PNA probe being used.

As can be gleaned from Figure 6 (curve B), no ECL emission is detected from the working electrode in absence of TPA. On addition of the co-reactant (Figure 6, curve C), a significant current corresponding to the oxidation of TPA and a strong ECL signal (Figure 6, curve A) from the Ru(II)-polypyridyl unit present in **PNA2** were simultaneously observed. A similar ECL-potential profile was also obtained from **PNA3** (data not shown). Note that the onset of the ECL emission occurred at the same potential as the onset of the oxidation of TPA which is prior to the oxidation of the attached Ru(II) moiety. It should also be noted that the ECL-potential profile displays two peaks (Figure 6, curve A). The peak at lower potential corresponds to the oxidation of the co-reactant while the one at higher potential is characteristic of the Ru(II) complex. Both the waves are associated with the emission from luminophoric $[Ru(bpy)_2(Cpp\text{-}L)]^{2+*}$ unit present in **PNA2** (and **PNA3**). An analogous behavior has previously been observed for other Ru(II) complexes and is believed to result from the action of parallel mechanisms producing the excited state.[38,63,64,69] These mechanisms are described in eqs 1−5 (vide supra) and 6−9:[38,63,64]

$$N(C_3H_7)_3 \rightleftharpoons N(C_3H_7)_3^{\bullet+} + e^- \quad (6)$$

$$N(C_3H_7)_3^{\bullet+} \rightleftharpoons CH_3CH_2C^{\bullet}HN(C_3H_7)_2 + H^+ \quad (7)$$

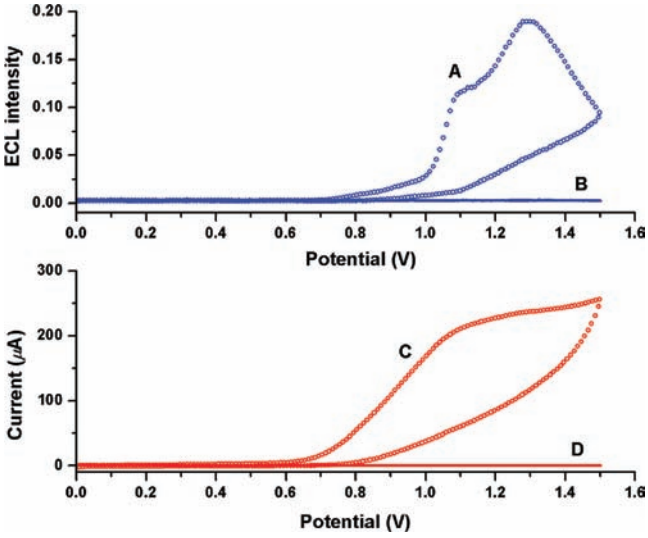


**Figure 6.** Cyclic voltammograms (bottom) and ECL response (top) of 0.1 $\mu$M **PNA2** in 0.1 M PBS buffer (pH 7.4) at a 3 mm diameter glassy carbon electrode using a scan rate of 100 mV $s^{-1}$. Curves A and C represent the responses in the presence of 0.1 M TPA while B and D represent the responses in the absence of the co-reactant.

$$CH_3CH_2C^{\bullet}HN(C_3H_7)_2 + [Ru(L)_3]^{2+} \rightleftharpoons [Ru(L)_3]^{+} + P \quad (8)$$

$$[Ru(L)_3]^{+} + N(C_3H_7)_3^{\bullet+} \rightleftharpoons [Ru(L)_3]^{2+*} + N(C_3H_7)_3 \quad (9)$$

followed by reaction 5 above.

The ability to generate intense ECL at low overpotentials is desirable as it decreases the likelihood of interfering side reactions, which would lower the ECL efficiency. The ECL emission seen from **PNA2** was more intense than that from **PNA3**, but both gave intensities approximately 10 times lower than observed from $[Ru(bpy)_3]^{2+}$ under the same conditions ($[Ru(bpy)_3]^{2+}$ > **PNA2** > **PNA3**). Duplex formation with the cDNA strand (**PNA2·DNA** and **PNA3·DNA**) also did not significantly affect the ECL intensity of the Ru(II)-PNA probe. Under the conditions described above for **PNA2** and **PNA3**, no ECL signal was detected from the solutions of nonmetalated PNA oligomers (**PNA1** and **PNA4**) or their corresponding **PNA·DNA** duplexes.

Although the ECL intensity observed from $[Ru(bpy)_3]^{2+}$ was more intense than for the novel Ru(II)-PNA oligomer systems, it should be noted that extremely low detection limits are still possible.[70] Thus, with even the submicromolar concentrations of Ru(II)-PNA sequences (**PNA2** and **PNA3**) used in these experiments, intense ECL signals well above the background were produced. These studies show the great potential of such Ru(II)-PNA oligomeric systems for ECL-based biosensing applications.

**Thermal Stability ($T_m$) of Ru(II)-PNA·DNA Duplexes.** UV melting experiments were carried out to assess the stability of duplexes formed by the Ru(II)-PNA sequences and their cDNA sequences. As noted above, an overhang of three thymine residues was provided on each end of the target DNA sequence. The UV melting curves recorded upon heating or cooling of equimolar mixtures in PBS solutions at pH 7.4 (UV-$T_m$) displayed a clear sigmoidal profile (Supporting Information,


dx.doi.org/10.1021/ic202761w | Inorg. Chem. 2012, 51, 3302−3315

**Table 5. Thermal Melting Temperatures ($T_m$) of PNA·DNA Duplexes**[a,b]

| PNA code | $T_m$ (°C)[c] | $\Delta T_m$ (°C)[d] |
|---|---|---|
| **PNA1** | 41.5 ± 0.7 | |
| **PNA2** | 49.1 ± 0.5 | 7.6 ± 0.9 |
| **PNA3** | 57.6 ± 0.2 | 16.1 ± 0.7 |
| **PNA4** | 53.6 ± 1.2 | 12.1 ± 1.4 |

[a]Hybridization studies were performed in 10 mM PBS buffer (pH 7.4) with equimolar PNA and DNA strand concentrations of 3 $\mu$M each. [b]Target DNA sequence: 5′-T-T-T-**T-T-T-T-A-T-T-G-C**-T-T-T-3′. [c]$T_m$ values were determined as the maxima of the first derivative plots of $A_{260}$ versus $T$ and are an average of four separate experiments ± standard deviation. [d]$\Delta T_m = T_m - T_m$ (PNA1).

Figures S16–S19). The experimentally calculated $T_m$ values for the **PNA·DNA** duplexes are summarized in Table 5. Notably, the $T_m$ values for the metal complex containing **PNA2·DNA** and **PNA3·DNA** duplexes were respectively 8 and 4 °C higher than for the corresponding metal-free duplexes (**PNA1·DNA** and **PNA4·DNA**, respectively) indicating that the inserted Ru(II) complex actually enhances the stability of the duplex. The four PNA sequences can be differentiated from each other on the basis of their overall positive charge, which arises from the poly lysine residues and cationic Ru(II) complex and increases in the order **PNA1** < **PNA2** < **PNA4** < **PNA3**. As expected, the stability of the respective **PNA·DNA** duplexes formed upon hybridization also increases with the increase in positive charge due to stronger electrostatic interactions with the negatively charged DNA backbone. Such an increase in the thermal stability of complementary **PNA·DNA** duplexes with an increase in the number of cationic residues on the PNA sequence has been noted by Brown and co-workers.[71] Our finding on the stability of the Ru-**PNA·DNA** duplex differs from the previous reports by Metzler-Nolte and co-workers on Ru-PNA/DNA binding.[43] In that study, however, bulky Ru(II) complexes were covalently attached on the terminal amino group of the PNA sequence, reducing the duplex stability by possible disruption of the neighboring A:T base pair. The dissimilarity in these results could be attributed to the fact that, in the systems reported here, the bulky Ru(II) complex is separated from the PNA backbone by a long linker, charged amino acid residues have been introduced, and a 3-nucleobase overhang has been added to the target DNA sequence.

**Circular Dichroism Spectroscopy.** The secondary structure of the **PNA·DNA** duplexes was also probed by means of CD spectroscopy. In general, the spectra of all **PNA·DNA** duplexes showed right handedness (Figure 7), consistent with the CD fingerprints of other **PNA·DNA** duplexes.[72] As expected, and also previously observed by Metzler-Nolte and coworkers,[24] the induction of the Ru(II) complex (a racemic mixture of two optically active Λ and Δ isomeric forms) into the PNA strand did not alter the helicity of the duplexes. The maxima located at about 260 nm for duplexes, **PNA1·DNA**, **PNA2·DNA**, and **PNA4·DNA**, was found to be substituted by a broad band existing at a slightly longer wavelength (270 nm) for **PNA3·DNA** duplex. On the basis of increased CD intensity for the band at 260 nm in **PNA4·DNA** relative to **PNA1·DNA** and **PNA2·DNA** and thermal melting temperatures, we can tentatively conclude that stronger $\pi-\pi$ interactions exist between the stacked nucleobases in the **PNA4·DNA** duplex. The difference in CD spectra for **PNA3·DNA** compared to others

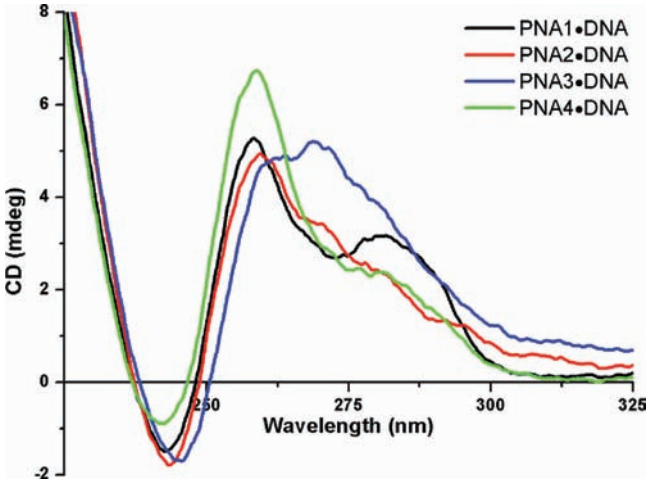


**Figure 7.** CD spectra of annealed Ru(II)-**PNA·DNA** duplexes (3 $\mu$M in 10 mM pH 7.4 PBS buffer).

suggests that its structure is distinctly different from the rest, implying significant influence from the inserted Ru(II)-polypyridyl units as well as the amino acid chain present on the respective PNA strand. Interestingly, in the absence of a conjugated peptide sequence no pronounced difference was observed between the CD spectra for the metal containing and nonmetalated **PNA·DNA** duplexes.

## CONCLUSION

We have expanded the library of Ru(II)-PNA like monomers to include three new Ru(II) complexes, $[Ru(bpy)_2(Cpp\text{-}L\text{-}PNA\text{-}OH)]^{2+}$ (**M1**), $[Ru(phen)_2(Cpp\text{-}L\text{-}PNA\text{-}OH)]^{2+}$ (**M2**), and $[Ru(dppz)_2(Cpp\text{-}L\text{-}PNA\text{-}OH)]^{2+}$ (**M3**), distinguishable on the basis of the degree of hydrophobicity and planarity of the three ancillary ligands, namely, dppz vs phen vs bpy. Their electronic absorption spectra exhibit MLCT and LC transition bands typical of $[Ru(tris)diimine]^{2+}$ complexes whereas the luminescence profiles obtained following 450 nm excitation display maxima between 635 and 665 nm. The formal oxidation potentials, $E^{\circ}_{f}$, systematically increase in the order bipyridyl (**M1**) < phenanthroline (**M2**) < dipyridophenazine (**M3**) derivative. The monomers showed intense ECL emission in the presence of co-reactant (TPA). A significant outcome of this work is the successful insertion of a Ru(II)-PNA monomer (**M1**) within the PNA sequence with the entire Ru(II)-PNA sequence constituted on the solid support. Incorporation into PNA sequences had relatively little effect on the electronic properties of the Ru(II)-tris(diimine) units and nor did the formation of duplexes with their cDNA sequences. Interestingly, UV melting experiments showed that hybrids formed by Ru(II)-containing PNA oligomers and cDNA sequences exhibit much higher thermal stability when compared to the nonmetalated **PNA·DNA** duplex. This can be attributed to additional positive charges introduced through the Ru(II) moiety and charged amino acid residues which result in stronger electrostatic interactions with the polyanionic DNA oligomer. Sequences **PNA2** and **PNA3**, as well as their corresponding **PNA·DNA** duplexes, showed significant ECL emission in the presence of co-reactant (TPA) even at submicromolar oligomer concentrations. The CD spectra indicated that the **PNA·DNA** duplexes exist in right handed helical form but that the structure of **PNA3·DNA** (duplex containing Ru(II) polypyridyl unit and NLS sequence) was distinctly different


dx.doi.org/10.1021/ic202761w | Inorg. Chem. 2012, 51, 3302–3315

from the other duplexes. In general, with the metal-PNA biosensing domain so far mainly dominated by ferrocenyl-PNA bioconjugate-based electrochemical biosenors,[7] we have demonstrated a method for designing Ru(II)-PNA bioconjugates, with available free sites for optional addition of amino acid residues for enhanced stability, solubility, and improved cellular uptakes. Such Ru(II)-PNA bioconjugates hold great potential for multimodal bionsensing applications.

## ■ ASSOCIATED CONTENT

### Supporting Information

Representative examples of $^1$H NMR spectra of **M1**−**M3** (Figures S1−S3); LC-MS spectra for **PNA1**, **PNA2**, **PNA3**, and **PNA4** (Figures S4−S7); MALDI-TOF spectra (Figures S8−S11); emission spectra for **M1**−**M3** (Figure S12); cyclic voltammograms of **M1**−**M3** as a function of scan rate (Figures S13−S15); voltammetric data (Table S1) and melting curves for **PNA1·DNA**, **PNA2·DNA**, **PNA3·DNA**, and **PNA4·DNA** duplexes (Figures S16−S19). This material is available free of charge via the Internet at http://pubs.acs.org.

## ■ AUTHOR INFORMATION

### Corresponding Author

*E-mail: leone.spiccia@monash.edu (L.S.), gilles.gasser@aci.uzh.ch (G.G.). Fax: +61 3 9905 4597 (L.S.), +41 44 635 68 03 (G.G.). WWW: http://www.chem.monash.edu.au/staff/spiccia/ (L.S.), www.gassergroup.com (G.G.).

### Notes

The authors declare no competing financial interest.

## ■ ACKNOWLEDGMENTS

This work was supported by the Australian Research Council through the Australian Centre of Excellence for Electromaterials Science (L.S.), the Swiss National Science Foundation (Ambizione Fellowship N° PZ00P2_126404, Professorship N° PP00P2_133568 and Research Grant N° 200021_129910 to G.G.) and the University of Zurich. P.S.F. acknowledges funding from the Australian Research Council (Future Fellowship) and Deakin University. T.J. is a recipient of Monash Graduate Scholarship and Monash International Postgraduate Research Scholarship. The authors are grateful to Ms. Anna Leonidova for her kind help with the MALDI-TOF measurements. G.G. thanks Prof. Roger Alberto for generous access to all the facilities of the Institute of Inorganic Chemistry of the University of Zurich.

## ■ REFERENCES

(1) Nielsen, P.; Egholm, M.; Berg, R.; Buchardt, O. *Science* **1991**, *254*, 1497.
(2) *Peptide Nucleic Acids, Protocols and Applications*; Nielsen, P. E., Egholm, M., Eds.; Horizon Scientific Press: Wymondham, U.K., 1999.
(3) Baldoli, C.; Cerea, P.; Giannini, C.; Licandro, E.; Rigamonti, C.; Maiorana, S. *Synlett* **2005**, *2005*, 1984.
(4) Ikeda, H.; Yoshida, K.; Ozeki, M.; Saito, I. *Tetrahedron Lett.* **2001**, *42*, 2529.
(5) Wilhelmsson, L. M.; Holmén, A.; Lincoln, P.; Nielsen, P. E.; Nordén, B. *J. Am. Chem. Soc.* **2001**, *123*, 2434.
(6) Wojciechowski, F.; Hudson, R. H. E. *Org. Lett.* **2009**, *11*, 4878.
(7) Gasser, G.; Sosniak, A. M.; Metzler-Nolte, N. *Dalton Trans.* **2011**, *40*, 7061 , and references therein.
(8) Bin, X.; Diakowski, P. M.; Kerman, K.; Kraatz, H.-B. In *Electrochemistry of Functional Supramolecular Systems*; John Wiley & Sons, Inc.: New York, 2010; p 261.
(9) Gao, L.; Li, C.; Li, X.; Kraatz, H.-B. *Chem. Commun.* **2010**, *46*, 6344.
(10) Li, C.; Li, X.; Liu, X.; Kraatz, H.-B. *Anal. Chem.* **2010**, *82*, 1166.
(11) Guo, K.; Li, X.; Kraatz, H.-B. *Biosens. Bioelectron.* **2011**, *27*, 187.
(12) Prencipe, G.; Maiorana, S.; Verderio, P.; Colombo, M.; Fermo, P.; Caneva, E.; Prosperi, D.; Licandro, E. *Chem. Commun.* **2009**, 6017.
(13) Stender, H. *Expert Rev. Mol. Diagn.* **2003**, *3*, 649.
(14) Forrest, G. N. *Expert Rev. Mol. Diagn.* **2007**, *7*, 231.
(15) Malic, S.; Hill, K. E.; Hayes, A.; Percival, S. L.; Thomas, D. W.; Williams, D. W. *Microbiology (Reading, U. K.)* **2009**, *155*, 2603.
(16) Koppelhus, U.; Awasthi, S. K.; Zachar, V.; Holst, H. U.; Ebbesen, P.; Nielsen, P. E. *Antisense Nucleic Acid Drug Dev.* **2002**, *12*, 51.
(17) Nielsen, P. E. *Q. Rev. Biophys.* **2005**, *38*, 345.
(18) Ferri, E.; Donghi, D.; Panigati, M.; Prencipe, G.; D'Alfonso, L.; Zanoni, I.; Baldoli, C.; Maiorana, S.; D'Alfonso, G.; Licandro, E. *Chem. Commun.* **2010**, *46*, 6255.
(19) Wang, J. In *Peptide Nucleic Acids, Protocols and Applications*; Nielsen, P. E., Egholm, M., Eds.; Horizon Scientific Press: Wymondham, U.K., 1999, p 155, and references therein.
(20) Maurer, A.; Kraatz, H.-B.; Metzler-Nolte, N. *Eur. J. Inorg. Chem.* **2005**, *2005*, 3207.
(21) Baldoli, C.; Rigamonti, C.; Maiorana, S.; Licandro, E.; Falciola, L.; Mussini, P. R. *Chem.—Eur. J.* **2006**, *12*, 4091.
(22) van Staveren, D. R.; Metzler-Nolte, N. *Chem. Rev.* **2004**, *104*, 5931 , and references therein.
(23) Metzler-Nolte, N. In *Bioorganometallics: Biomolecules, Labeling, Medicine*; Jaouen, G., Ed.; Wiley-VCH: Weinheim, Germany, 2006, p 125.
(24) Gasser, G.; Husken, N.; Koster, S. D.; Metzler-Nolte, N. *Chem. Commun.* **2008**, 3675.
(25) Baldoli, C.; Oldani, C.; Licandro, E.; Ramani, P.; Valerio, A.; Ferruti, P.; Falciola, L.; Mussini, P. *J. Organomet. Chem.* **2007**, *692*, 1363.
(26) Gasser, G.; Brosch, O.; Ewers, A.; Weyhermüller, T.; Metzler-Nolte, N. *Dalton Trans.* **2009**, 4310.
(27) Patra, M.; Gasser, G.; Bobukhov, D.; Merz, K.; Shtemenko, A. V.; Metzler-Nolte, N. *Dalton Trans.* **2010**, *39*, 5617.
(28) Gasser, G.; Neumann, S.; Ott, I.; Seitz, M.; Heumann, R.; Metzler-Nolte, N. *Eur. J. Inorg. Chem.* **2011**, *36*, 5471.
(29) Hüsken, N.; Gasser, G.; Köster, S. D.; Metzler-Nolte, N. *Bioconjugate Chem.* **2009**, *20*, 1578.
(30) Sosniak, A.; Gasser, G.; Metzler-Nolte, N. *Org. Biomol. Chem.* **2009**, *7*, 4992.
(31) Juris, A.; Balzani, V.; Barigelletti, F.; Campagna, S.; Belser, P.; von Zelewsky, A. *Coord. Chem. Rev.* **1988**, *84*, 85.
(32) Spiccia, L.; Deacon, G. B.; Kepert, C. M. *Coord. Chem. Rev.* **2004**, *248*, 1329.
(33) Zhou, M.; Robertson, G. P.; Roovers, J. *Inorg. Chem.* **2005**, *44*, 8317.
(34) Gorman, B. A.; Francis, P. S.; Barnett, N. W. *Analyst* **2006**, *131*, 616.
(35) Fernández-Moreira, V.; Thorp-Greenwood, F. L.; Coogan, M. P. *Chem. Commun.* **2010**, *46*, 186 , and references therein.
(36) Forster, R. J.; Bertoncello, P.; Keyes, T. E. *Annu. Rev. Anal. Chem.* **2009**, *2*, 359.
(37) Miao, W. *Chem. Rev.* **2008**, *108*, 2506.
(38) Bard, A. J. *Electrogenerated Chemiluminescence*; Marcel Dekker: New York, 2004.
(39) Barbante, G. J.; Hogan, C. F.; Wilson, D. J. D.; Lewcenko, N. A.; Pfeffer, F. M.; Barnett, N. W.; Francis, P. S. *Analyst* **2011**, *136*, 1329.
(40) Zhao, Q.; Huang, C.; Li, F. *Chem. Soc. Rev.* **2011**, *40*, 2508.
(41) Puckett, C. A.; Ernst, R. J.; Barton, J. K. *Dalton Trans.* **2010**, *39*, 1159.
(42) Puckett, C. A.; Barton, J. K. *Bioorg. Med. Chem.* **2010**, *18*, 3564.
(43) Verheijen, J. C.; van der Marel, G. A.; van Boom, J. H.; Metzler-Nolte, N. *Bioconjugate Chem.* **2000**, *11*, 741.
(44) Nickita, N.; Gasser, G.; Bond, A. M.; Spiccia, L. *Eur. J. Inorg. Chem.* **2009**, *2009*, 2179.
(45) Joshi, T.; Barbante, G. J.; Francis, P. S.; Hogan, C. F.; Bond, A. M.; Spiccia, L. *Inorg. Chem.* **2011**, *50*, 12172.

(46) Shiraishi, T.; Nielsen, P. E. In *Delivery Technologies for Biopharmaceuticals*; John Wiley & Sons, Ltd: New York, 2009; p 305.
(47) Kissinger, T.; Heineman, W. R. In *Laboratory Techniques in Electroanalytical Chemistry*, 2nd ed.; Marcel Dekker Inc.: New York: 1996; p 469.
(48) Gottlieb, H. E.; Kotlyar, V.; Nudelman, A. *J. Org. Chem.* **1997**, *62*, 7512.
(49) Nickita, N.; Gasser, G.; Pearson, P.; Belousoff, M. J.; Goh, L. Y.; Bond, A. M.; Deacon, G. B.; Spiccia, L. *Inorg. Chem.* **2008**, *48*, 68.
(50) Greguric, A.; Greguric, I. D.; Hambley, T. W.; Aldrich-Wright, J. R.; Collins, J. G. *J. Chem. Soc., Dalton Trans.* **2002**, 849.
(51) Anderson, P. A.; Deacon, G. B.; Haarmann, K. H.; Keene, F. R.; Meyer, T. J.; Reitsma, D. A.; Skelton, B. W.; Strouse, G. F.; Thomas, N. C. *Inorg. Chem.* **1995**, *34*, 6145.
(52) Bischof, C.; Joshi, T.; Weiß, J.; Ehrlich, M.; Spiccia, L.; Schatzschneider, U. *Inorg. Chem.* **2011**, submitted for publication.
(53) Gasser, G.; Sosniak, A. M.; Leonidova, A.; Braband, H.; Metzler-Nolte, N. *Aust. J. Chem.* **2011**, *64*, 265.
(54) Gasser, G.; Jäger, K.; Zenker, M.; Bergmann, R.; Steinbach, J.; Stephan, H.; Metzler-Nolte, N. *J. Inorg. Biochem.* **2010**, *104*, 1133.
(55) Gasser, G.; Pinto, A.; Neumann, S.; Sosniak, A. M.; Seitz, M.; Merz, K.; Heumann, R.; Metzler-Nolte, N. *Dalton Trans.* **2012**, *41*, 2304.
(56) Thomson, S. A.; Josey, J. A.; Cadilla, R.; Gaul, M. D.; Hassman, C. F.; Luzzio, M. J.; Pipe, A. J.; Reed, K. L.; Ricca, D. J.; Wiethe, R. W.; Noble, S. A. *Tetrahedron* **1995**, *51*, 6179.
(57) Kalderon, D.; Roberts, B. L.; Richardson, W. D.; Smith, A. E. *Cell* **1984**, *39*, 499.
(58) Mayfield, L. D.; Corey, D. R. *Bioorg. Med. Chem. Lett.* **1999**, *9*, 1419.
(59) Nickita, N.; Belousoff, M. J.; Bhatt, A. I.; Bond, A. M.; Deacon, G. B.; Gasser, G.; Spiccia, L. *Inorg. Chem.* **2007**, *46*, 8638.
(60) Bard, A. J.; Faulkner, L. R. *Electrochemical Methods, Fundamentals and Application*, 2nd ed.; Wiley: Brisbane, Australia, 2001.
(61) Sevick, A. *Collect. Czech. Chem. Commun.* **1948**, *13*, 349.
(62) Randles, J. E. B. *Trans. Faraday Soc.* **1948**, *44*, 327.
(63) Miao, W.; Choi, J.-P.; Bard, A. J. *J. Am. Chem. Soc.* **2002**, *124*, 14478.
(64) Wightman, R. M.; Forry, S. P.; Maus, R.; Badocco, D.; Pastore, P. *J. Phys. Chem. B* **2004**, *108*, 19119.
(65) Leland, J. K.; Powell, M. J. *J. Electrochem. Soc.* **1990**, *137*, 3127.
(66) Barbante, G. J.; Hogan, C. F.; Mechler, A.; Hughes, A. B. *J. Mater. Chem.* **2010**, *20*, 891.
(67) Cooke, M. M.; Doeven, E. H.; Hogan, C. F.; Adcock, J. L.; McDermott, G. P.; Conlan, X. A.; Barnett, N. W.; Pfeffer, F. M.; Francis, P. S. *Anal. Chim. Acta* **2009**, *635*, 94.
(68) Hess, A.; Metzler-Nolte, N. *Chem. Commun.* **1999**, 885.
(69) Zu, Y.; Bard, A. J. *Anal. Chem.* **2000**, *72*, 3223.
(70) Arora, A.; J. de Mello, A.; Manz, A. *Anal. Commun.* **1997**, *34*, 393.
(71) Silvester, N. C.; Bushell, G. R.; Searles, D. J.; Brown, C. L. *Org. Biomol. Chem.* **2007**, *5*, 917.
(72) Egholm, M.; Buchardt, O.; Christensen, L.; Behrens, C.; Freier, S. M.; Driver, D. A.; Berg, R. H.; Kim, S. K.; Norden, B.; Nielsen, P. E. *Nature* **1993**, *365*, 566.